Physics OCT 1957 21

REGISTERED No. M. 3121

UNIVERSITY OF MICHIGAN
OCT 17 1957
PHYSICS LIBRARY

PROCEEDINGS
OF THE
INDIAN ACADEMY
OF SCIENCES

VOL. XLVI] *SECTION A* [No. 2

AUGUST 1957

Price Rs. 2 or 3 Sh. *Annual Subscription Rs. 18*

THE USE OF ANOMALOUS SCATTERING FOR THE DETERMINATION OF CRYSTAL STRUCTURES—$KMnO_4$

By S. Ramaseshan, F.A.Sc., K. Venkatesan and N. V. Mani

(Department of Physics, Indian Institute of Science, Bangalore-3)

Received May 10, 1957

1. Introduction

It is well known that when the frequency of the incident radiation is very close to that of the absorption edge of an atom, it scatters anomalously. The anomalous scattering makes itself felt in two ways; firstly by a decrease in the real part of the scattering factor, and secondly by an introduction of a phase-lag during the scattering process. The former effect manifests itself irrespective of whether the frequency of the incident radiation (ν) is smaller or larger than that of the absorption edge (ν_a), whereas the latter effect exists only when $\nu > \nu_a$ (James, 1948). This phase change during anomalous scattering is mainly responsible for the failure of the Friedel's law in non-centrosymmetric structures and has been used in a most elegant manner for the determination of the absolute configuration of non-centrosymmetric crystals (Bijvoet, 1954). Significant advance has recently been made in this method for the direct evaluation of the phases of the structure amplitudes by Ramachandran and Raman (1956) and by Okaya, Saito and Pepinsky (1955).

In this paper we shall concern ourselves only with the first effect, *i.e.*, the decrease in the real part of the scattering factor of an anomalously scattering atom. It is quite obvious that this effect can be used to great advantage in the direct determination of structures of crystals. For example, the relative intensity data obtained for a crystal with X-rays having wavelengths very far from the absorption edge of the atoms, would necessarily be different from those obtained with the incident radiation having a wavelength close to an absorption edge of one of the atoms. This difference, although very small, is very well within the limits of experimental determination and has been measured to a fair degree of accuracy by different authors (James, 1948).

The use of two appropriate wavelengths with one crystal would in effect, be equivalent to the substitution of one of the atoms of the crystal by an atom of slightly different scattering power. Consequently, all the methods and techniques that are applicable to the isomorphous replacement method can

be used. There have been a few attempts to make use of the anomalous scattering for structure determination. Particular mention may be made of the work of Bradley and Rodgers (1934) in the determination of the structure of Heusler alloys and that of Jones and Sykes (1937) in establishing the super-lattice structure of copper-zinc alloys. Although this technique has long been thought of by many (*see* for example *The Crystalline State*, Vol. III, p. 227) it has never been used for solving a structure or for the determination of the signs of the structure factors. It is the purpose of this paper to show that the anomalous scattering method is practicable and can be used with success at least in the case of relatively simple structures.

The substance used in this investigation is $KMnO_4$. The choice of the substance was governed by many factors. The primary one was that the Mn atom gave the maximum decrease in the real part of the scattering factor for the radiations most readily available in this laboratory (copper, cobalt and iron). Further at the commencement of this investigation it was thought that as the structure of this crystal had been solved (Mooney, 1931) the practicability or otherwise of this technique could be decided quite easily. Unfortunately, a careful study of the literature (Wyckoff, 1935) revealed that the published atomic parameters for $KMnO_4$ were by no means accurate, thus necessitating a complete redetermination of the structure.

Potassium permanganate belongs to the orthorhombic space group *Pnma* with cell dimensions $a = 9{\cdot}09$ Å, $b = 7{\cdot}41$ Å, $c = 5{\cdot}72$ Å, with four molecules per unit cell.

2. Experimental Procedure

From the remarks made above, the procedure to be followed for obtaining the data for structure computations would be the following:—(i) to choose the appropriate radiations for the particular crystal under study, (ii) using these to obtain satisfactory Weissenberg photographs and to measure the intensities of all the recorded reflexions, (iii) to make the proper corrections for geometrical and physical factors and finally (iv) to reduce the data obtained with the two radiations to the same relative scale.

The success of the investigation would largely depend on the preciseness with which each of these operations can be carried out. For example, any inaccuracy in the reading of the intensity or in the application of the absorption correction may completely mask the comparatively small differences in the relative intensities caused by the anomalous scattering of one of the atoms.

It would obviously be most advantageous to use two radiations for which the anomalous scattering atom (Mn in the present case) exhibits the maximum

difference in scattering power. The scattering factor f of an atom is given by

$$f = f_\theta + \Delta f' + i\,\Delta f'' \qquad (1)$$

TABLE I (*a*)

$\Delta f'$ and $\Delta f''$ for manganese for CuKα, CoKα and FeKα f_0 for Mn is 25. *The K-absorption edge of Mn*.....1·895 Å

Radiation	λ_i	λ_i/λ_k	$-\Delta f'$	$\Delta f''$
CuKα ..	1·541 Å	0·813	0·789	2·63
CoKα ..	1·789	0·944	2·62	3·34
FeKα ..	1·936	1·021	4·21	0·00

TABLE I (*b*)

Values of $|f|$ for Mn, K and O for different values of $\sin\theta/\lambda$

$10^{-8}\times \frac{\sin\theta}{\lambda}$ / $\lvert f\rvert$	0·0	0·1	0·2	0·3	0·4	0·5	0·6
f^{Mn}_{Cu}	24·4	21·5	17·6	14·4	12·2	10·6	9·3
f^{Mn}_{Fe}	20·2	17·9	15·9	10·7	8·5	6·9	5·5
f^{Mn}_{Co}	22·7	19·8	14·0	12·7	10·6	9·1	7·8
f^{K}	18·0	16·5	13·3	10·8	8·9	7·8	7·1
f^{O}	8·0	7·1	5·3	3·9	2·9	2·2	1·8

where f_θ is the scattering factor for waves short in comparison with the wavelength of the absorption edge of the scattering element and $\Delta f'$ and $\Delta f''$ are the real and the imaginary parts of the corrections to be applied to the scattering factor on account of the dispersion effects. The values of these scattering constants for manganese for CuK_α, CoK_α and FeK_α calculated on the basis of Honl's theory are given in Table I *a*. The absence of the phase-lag for FeK_α (*i.e.*, $\Delta f'' = 0$) must be noted. Further, since f_θ is a decreasing function of $\sin\theta/\lambda$ and $\Delta f'$ and $\Delta f''$ are for most practical purposes independent of the angle of scattering, the effect of anomalous scattering is most evident for large

values of θ. The scattering factor $| f |$ for Mn for the three wavelengths for different values of $\sin\theta/\lambda$ are given in Table I *b*. The scattering factors for potassium and oxygen have also been entered in this table. It has been assumed that as the three radiations used are quite away from the absorption edge of these atoms, their scattering factors are independent of the incident frequency. It must be mentioned that although data using the K_α radiations of Cu, Co and Fe were recorded, most of the computations were made using those for CuK_α and FeK_α.

Using a cylindrical specimen having diameter less than 0·08 mm., multiple film zero-layer Weissenberg photographs about the *b*-axis (*hol*) were taken with copper K_α, cobalt K_α and Iron K_α radiations. Although there was a considerable amount of fluorescence, particularly for the first two radiations, the first film in the stack served as an efficient filter. The intensity was, therefore, measured from the second film onwards. Care was taken to adjust the times of exposure to compensate for the considerable differences in the absorption coefficients of the crystal and of the film for the three radiations.

The intensities were estimated visually, the comparison being made with a standard scale independently by the three investigators. The film factor for each of the three radiations was also determined accurately and it was found to follow the λ^{-3} law fairly well. The relative intensities were corrected for Lorentz and polarisation factors and also for absorption, using Bradley's table for cylindrical specimens.

The (*hko*) data were obtained only for CuK_α and the (*hol*) and (*hko*) data for $KClO_4$ were also recorded for the same radiation.

The next important problem is to put the data obtained with the different radiations on the same relative scale. This becomes significant particularly when " difference techniques " are adopted. For example, when a difference Patterson projection is made, if the relative scaling is not perfect, the map would be superposed on a faint Patterson which, by the introduction of more peaks, would very much complicate the interpretation.

A modification of the Wilson's method similar to the one suggested by Harker (1956) was used. The equation

$$C\frac{\langle I_{Cu}\rangle}{\langle I_{Fe}\rangle} = \frac{\sum_{r=1}^{N}\langle {}_{Cu}f_r^2\rangle}{\sum_{r=1}^{N}\langle {}_{Fe}f_r^2\rangle} \qquad (2)$$

was employed in the estimation of the scale factor C. Here $\langle I_{Cu}\rangle$ and $\langle I_{Fe}\rangle$ are the average intensities over particular ranges of $\sin^2\theta/\lambda^2$ and $\langle f_r\rangle$ the corresponding values of the scattering factors of all the representative atoms.

This method proves eminently successful as the *relative scale factor* between copper and iron data obtained by this method was correct to within 2% of the final value found at the completion of the investigation, although the *absolute scale factor* had to be altered by a considerable extent during the structure determination.

3. The Anomalous Difference Patterson

When the X-ray diffraction data for a pair of isomorphous crystals are available, perhaps the simplest method of utilising this data for a direct solution of the structure is the " Difference Patterson " technique. This method first suggested by Buerger (1942) has been thoroughly investigated by Kartha and Ramachandran (1955). The method consists of making a Patterson with $(|F_{M_1}|^2 - |F_{M_2}|^2)$ as coefficient, where M_1 and M_2 refer to the two isomorphous crystals. The peaks in such a diagram represent the interactions between the replaceable atoms themselves and also those between the replaceable atoms and the rest of the atoms in the structure, while the interactions between the non-replaceable atoms get cancelled out. This considerably reduces the number of peaks present, thus facilitating the interpretation. The symmetries introduced into this Difference Patterson due to the very nature of the Patterson function together with the symmetry of the replaceable atoms themselves have been most exhaustively treated in the paper by Kartha and Ramachandran cited above and will therefore not be dealt with here. Suffice it to say that in the most general case it is essential to know the positions of the replaceable atoms if the complete structure is to be obtained from the Difference Patterson diagram. Once the co-ordinates of the replaceable atoms are known, the correct structure can be obtained using Buerger's minimum function method (Buerger, 1951).

It is quite evident that the above methods can be directly applied when accurate intensity data are available for the same crystal with two wavelengths which are scattered anomalously by one set of atoms in the crystal; for in this case an exact isomorphism can be realized. With the (*hol*) data obtained for $KMnO_4$ with CuK_α, and FeK_α, a Difference Patterson map was computed with $(|F_{Cu}|^2 - |F_{Fe}|^2)$ as coefficient. Since the total number of reflexions observed with CuK_α for this zone was 90 and that obtained with FeK_α was only 60, the Difference Patterson could only be made using these 60 reflexions and the diagram obtained is given in Fig. 1. To see whether this map has any significance at all a Difference Patterson given in Fig. 2 was made using $(|F_{Cu}^{KMnO_4}|^2 - |F_{Cu}^{KClO_4}|^2)$ as coefficient. The striking similarity between the Anomalous Difference Patterson (A.D.P.) and the Isomorphous Difference Patterson (I.D.P.) was most gratifying and it indicated without any doubt

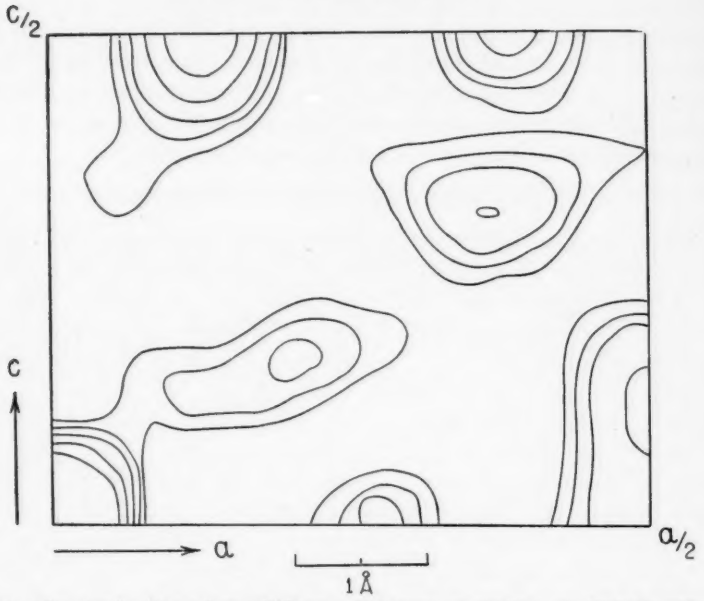

FIG. 1. The *b*-axis Anomalous Difference Patterson projection of $KMnO_4$ with $(|F_{Cu}|^2 - |F_{Fe}|^2)$ as coefficient.

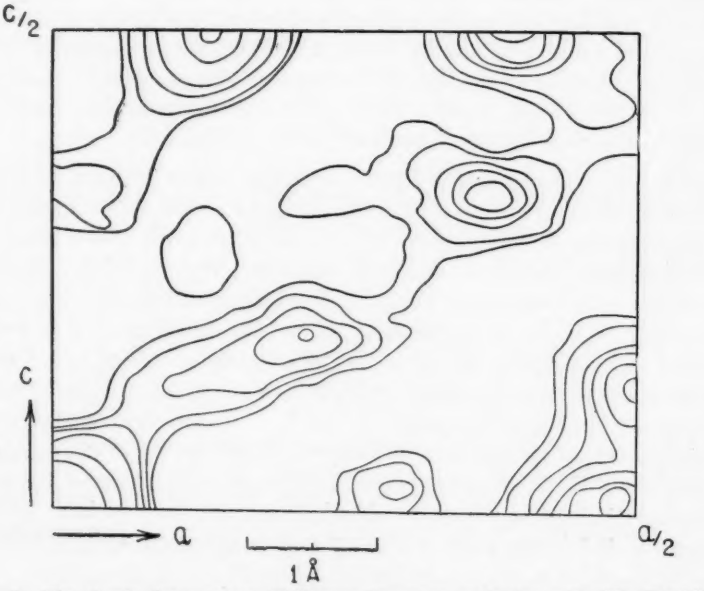

FIG. 2. The *b*-axis Isomorphous Difference Patterson projection with $(|F_{Cu}{}^{KMnO_4}|^2 - |F_{Cu}{}^{KClO_4}|^2)$ as coefficient.

that the anomalous technique can be used with success, at least for this particular structure. It may be remarked that it was rather difficult to distinguish between the Mn-Mn peak and the Mn-2 (0) peak in the simple Patterson projection. But this ambiguity was completely removed in the A.D.P. map because of the considerable enhancement of the peak due to the Mn-Mn interaction.

Knowing the Mn-Mn peaks the complete structure can be recovered, as has been remarked earlier, by the use of Buerger's minimum function method. This is done by drawing contours corresponding to the lower of the two values in two superposed A.D.P. diagrams, one translated with respect to the other in such a manner that the origin of one was on one of the identifiable atoms of the other. Figure 3 represents the minimum function diagram obtained after two translations. The different atoms of the $KMnO_4$ structure can be easily identified. These atomic co-ordinates could well be the starting point for the refinement of the parameters by the Fourier synthesis method. But before proceeding to refine the atomic parameters we shall investigate whether the position of the anomalously scattering atom can be determined by a direct method and, if so, whether the signs of the structure factors can also be evaluated.

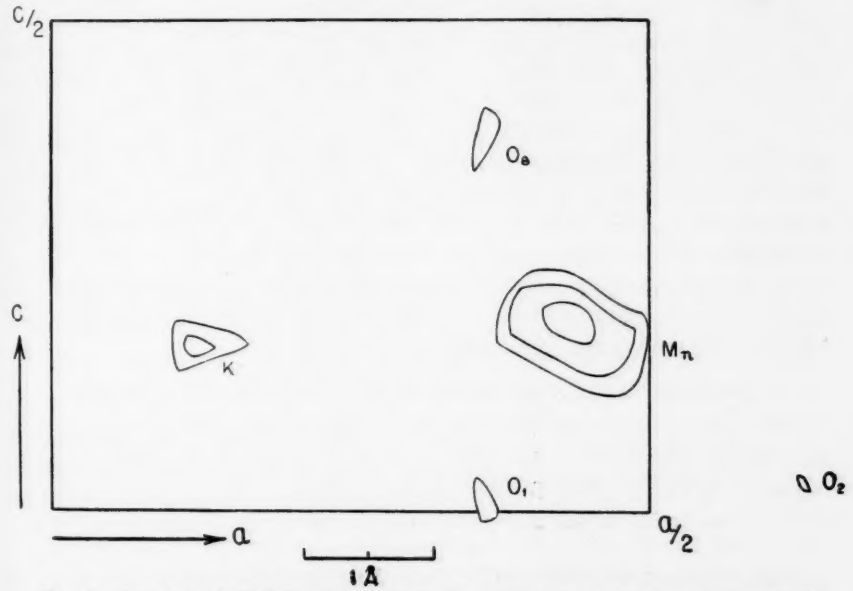

FIG. 3. Structure of $KMnO_4$ derived from the A.D.P. by Buerger's minimum function method.

4. Position of the Anomalously Scattering Atom

The Harker section of the A.D.P. diagram can be used to fix the position of the excited atom because this map will contain only the excited atom interactions, apart from accidental non-Harker peaks [Buerger (1942); Kartha and Ramachandran (1955)]. Instead, the positions of the anomalous scatterers can be determined directly by making a Patterson projection with $(|F_{Cu}| - |F_{Fe}|)^2$ as coefficient.* The corresponding function for isomorphous replacement was first used by Frueh (1953) for a different purpose and has been called by him the " Patterson function of the difference structure ". In the equation for centrosymmetric crystals

$$(F_{Cu} - F_{Fe}) = \sum_j (f_j^{Cu} - f_j^{Fe}) \cos 2\pi (hx_j + ky_j + lz_j)$$

the right-hand-side exists only for the anomalously scattering atoms. Hence the Patterson using $(F_{Cu} - F_{Fe})^2$ corresponds to the interaction due to the anomalously scattering atoms only. Since one does not know the signs of F_{Cu} and F_{Fe} there would be some difficulty. By the very nature of the function, $(|F_{Cu}| - |F_{Fe}|)^2 = (F_{Cu} - F_{Fe})^2$ when F_{Cu} and F_{Fe} are of the same sign. If, however, the two are of different signs the value of the coefficient used will be different. For most practical purposes in the present case, $f_{Cu} - f_{Fe} \simeq 4$ and so the number of reflexions wherein there would be such a change in sign would be very small indeed. Even here such a reflexion is not completely omitted from the calculation but a slightly different weight for the reflexion is used. This should hardly affect the position of the peaks. Figure 4 gives the projection made with $(|F_{Cu}| - |F_{Fe}|)^2$ as coefficient. The position of the anomalously scattering atom can be directly obtained from the map. The other faint peaks corresponding to other interactions (*cf.* Anomalous Difference Patterson in Fig. 1) appear because of one or more of the following reasons: (*a*) errors in the measurement of the intensities, (*b*) errors due to differences in extinctions of the intense reflexions for the different radiations and (*c*) error in the scale factor. In spite of these errors the positions of the Mn-Mn interactions are quite unmistakable.

5. Determination of the Signs of the Structure Factors

Once the position of the anomalously scattering atom is determined, it must be possible to obtain the signs of the structure amplitudes by the method suggested by Booth (1948) for isomorphous crystals. If j represents the anomalously scattering atoms and p the other atoms in the structure and if F_{Cu}

* The authors are most grateful to Dr. Gopinath Kartha for drawing their attention to this extremely useful function.

and F_{Fe} are the structure factors for CuK_α and FeK_α then for a centrosymmetric crystal,

$$\pm F_{Cu} = \sum_j f_j^{Cu} \cos 2\pi (hx_j + ky_j + lz_j) + \sum_p f_p^{Cu} \cos 2\pi (hx_p + ky_p + lz_p) \quad (3)$$

$$\pm F_{Fe} = \sum_j f_j^{Fe} \cos 2\pi (hx_j + ky_j + lz_j) + \sum_p f_p^{Fe} \cos 2\pi (hx_p + ky_p + lz_p) \quad (4)$$

Since $f_p^{Cu} = f_p^{Fe}$ and $f_j^{Cu} \neq f_j^{Fe}$

$$(\pm F_{Cu}) - (\pm F_{Fe}) = \sum_j (f_j^{Cu} - f_j^{Fe}) \cos 2\pi (hx_j + ky_j + lz_j) \quad (5)$$

For the (*hol*) reflexions of the space group *Pnma* equation (5) reduces to

$$(\pm F_{Cu}) - (\pm F_{Fe}) = 4 \sum_j (f_j^{Cu} - f_j^{Fe}) \cos 2\pi hx_j \cos 2\pi lz_j \quad (6)$$

$$\text{for } h + l = 2n \text{ and}$$

$$(\pm F_{Cu}) - (\pm F_{Fe}) = -4 \sum_j (f_j^{Cu} - f_j^{Fe}) \sin 2\pi hx_j \sin 2\pi lz_j \quad (7)$$

$$\text{for } h + l = 2n + 1$$

Since the positions of the anomalously scattering atoms are known (*see* previous section) the trigonometric part of equation can be computed. Further as f_j^{Cu} and f_j^{Fe} are known the signs of F_{Cu} or F_{Fe} can be fixed by inspection. In the present case $f^{Cu} - f^{Fe} \simeq 4$ and using equations (6) and (7), it was possible to determine the signs of as many as 50% of the reflexions recorded with CuK_α (*i.e.*, 75% of the reflexions recorded with FeK_α). The structure factors whose signs could be unambiguously determined have been indicated in Table IV. From this the determination of the structure and the refinement of the parameters is almost a routine procedure.

6. Refinement of the Parameters

Only the barest details of the determination of the structure will be given in this section. For any further details one may refer to the forthcoming papers on the structure of NH_4ClO_4 and $KClO_4$ by two of the present writers (K. V. and N. V. M.). Since $KMnO_4$ belongs to the space group *Pnma*, the K, Mn and two oxygen atoms lie on the symmetry planes. It is, therefore, necessary to determine only the x and z co-ordinates for these atoms while all the three co-ordinates have to be found for the two remaining oxygens which lie on either side of the symmetry plane.

The x and z co-ordinates are determined from the b-axis data. The first (*hol*) Fourier projection was made with 42 structure factors whose signs were determined by the method indicated in the previous section,

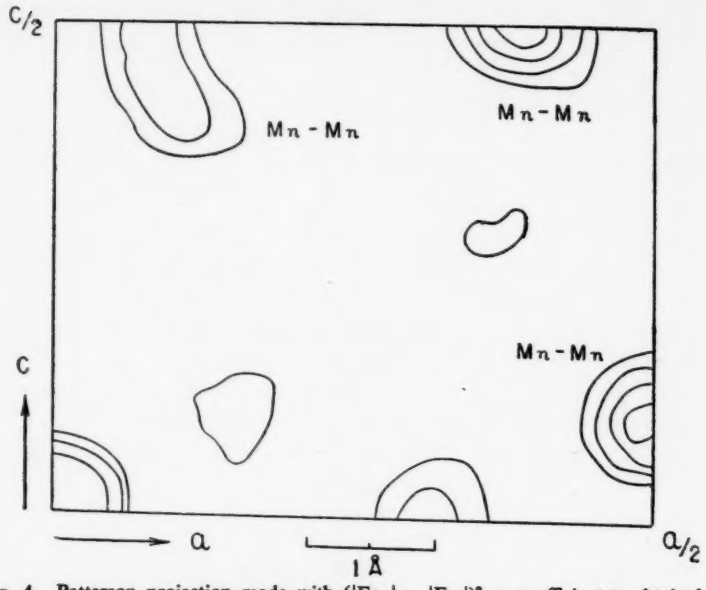

FIG. 4. Patterson projection made with $(|F_{Co}| - |F_{Fe}|)^2$ as coefficient to obtain the position of the anomalously scattering atom.

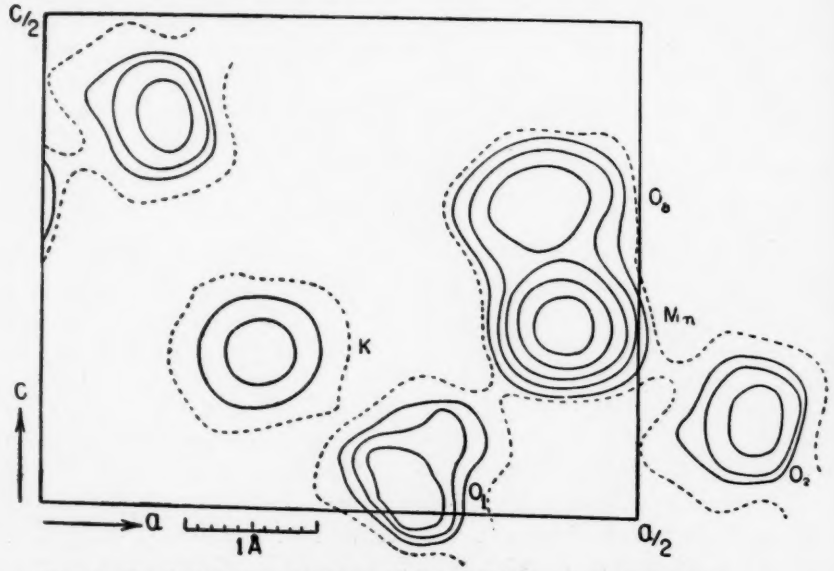

FIG. 5. The final electron density projection of $KMnO_4$ on the (010) plane.

Subsequent refinement of x and z parameters was carried out by the iterative process of Fourier and difference syntheses. At each stage the scale and temperature factors were estimated. A correction was applied for the few reflexions which were obviously affected by extinction effects. The final (*hol*) projection is given in Fig. 5. The R-factor for this projection was 0·145 (omitting a few unobservable reflexions).

The only other parameter that remains to be determined is the y parameter of the oxygen atoms off the symmetry plane. An approximate order of this co-ordinate was first estimated by assuming the MnO_4 group to be nearly a regular tetrahedron. The refinement of this parameter was carried out by the method of least squares, a method most suitable in this case as there were only 30 reflexions in this projection. The R-factor for this zone was 0·153 (removing the three most intense reflexions 020, 040 and 210 which suffer extinction effects). Table II gives the final parameters of the different atoms together with those reported by Mooney referred to the centre of

TABLE II

The final atomic parameters in fractional co-ordinates

Atom	Present work			Previous work		
	x	y	z	x	y	z
Potassium ..	0·183	0·750	0·158	0·185	0·750	0·160
Manganese ..	0·438	0·250	0·192	0·445	0·250	0·170
Oxygen 1 ..	0·321	0·250	0·038	0·365	0·250	−0·010
Oxygen 2 ..	0·594	0·250	0·106	0·625	0·250	0·110
Oxygen 3 ..	0·417	0·037	0·317	0·435	0·030	0·300
Oxygen 4 ..	0·417	0·463	0·317	0·435	0·470	0·300

symmetry as the origin. Significant differences particularly in the positions of the oxygens atoms (O_1 and O_2) can be noticed. Table III gives the different atomic distances in the MnO_4 group. It is rather difficult to determine the order of the errors present in the values given in Table III because of the presence of two heavy atoms in the asymmetric unit. It is estimated that the Mn–O distance will be correct to within 5%. The R-factor for the structure

TABLE III

Interatomic distances in $KMnO_4$ structure

Atoms	Present work	Previous work
$Mn—O_1$ ..	1·56 Å	1·69 Å
$Mn—O_2$ ..	1·56	1·52
$Mn—O_3$ ..	1·54	1·58
$Mn—O_4$ ..	1·54	1·58
$O_1—O_2$ ..	2·53	2·54
$O_2—O_3$ ..	2·55	2·62
$O_1—O_3$ ..	2·55	2·70
$O_3—O_4$ ..	2·44	2·53

with the K and Mn contributions removed is about 30%. The observed structure factors and those calculated using the final atomic positions for (*hol*) reflexions for the three radiations are given in Table IV and Table V gives the corresponding quantities for (*hko*) reflexions. Table VI gives the discrepancy factors.

7. CONCLUDING REMARKS

It is clear that if the structure is accurately known, one could reverse the process and compute the experimental scattering curve for the anomalously scattering atom for the different incident radiations. This would involve assuming a knowledge of the scattering factor curves for the non-anomalously scattering atoms. Even in the present investigation there are some indications that for Iron radiation $\triangle f'$ for Mn is not quite independent of the angle of the scattering. More accurate experimentation is necessary before one could assert this.

It is not necessary to deal here specifically with the properties of the Anomalous Difference Patterson for it behaves practically as the Isomorphous Difference Patterson does. Probably the only significant difference between the two will be the considerably greater amount of diffraction or termination errors that would exist in the former. This arises because $(f_{Cu} - f_{Fe})$ is practically constant and not a decreasing function of θ as it is in isomorphous case,

TABLE IV

Observed and calculated values of the structure factor for the (hol) reflexions of $KMnO_4$ for CuK_α, FeK_α and CoK_α

h o	F_0Cu	F_cCu	F_0Fe	F_cFe	F_0Co	F_cCo	*h o l*	F_0Cu	F_cCu	F_0Fe	F_cFe	F_0Co	F_cCo
1	2	3	4	5	6	7	8	9	10	11	12	13	14
0 0 2†	80·4	−88·9	70·6	−77·6	75·2	−83·3	9 0 1	VVW	<1	..	..	..	..
0 0 4†	23·9	−27·3	26·1	−29·5	24·9	−28·5	9 0 3	4·0	5·5	..	..	..	..
0 0 6†	61·0	51·7	47·8	45·2	50·4	48·5	9 0 5	15·7	15·7	..	..	..	..
0 0 8	26·7	−27·6	..	..	..	..							
							2 0 1†	47·9	45·3	36·5	38·7	40·5	43·3
2 0 0†	44·0	40·4	28·3	28·5	32·4	33·6	2 0 3†	44·8	−41·5	35·9	−36·7	37·9	−39·0
4 0 0	40·6	−40·3	37·8	−40·0	41·5	−40·2	2 0 5	16·1	13·3	15·8	16·1	11·7	15·0
6 0 0†	24·3	−25·3	12·7	−16·0	18·4	−20·7	2 0 7	18·2	23·6	20·5	19·0	18·3	21·3
8 0 0	49·9	−63·7	46·7	−54·3	51·8	−59·6	2 0 9	15·5	15·4	..	..	..	..
10 0 0	VVW	∼0	..	..	..	..							
							4 0 1†	102·0	108·6	84·5	94·9	92·3	101·4
2 0 2†	58·6	−48·4	45·8	−40·5	46·7	−44·2	4 0 3†	49·2	−38·8	37·0	−31·4	40·5	−35·1
2 0 4†	14·1	11·4	6·8	10·5	9·3	11·0	4 0 5†	48·2	−45·1	32·4	−36·1	42·2	−43·1
2 0 6†	VVW	1·8	3·3	− 2·2	8·4	<1	4 0 7	30·2	35·1	..	..	..	..
2 0 8	13·5	15·7	..	..	..	..	4 0 9	VVW	3·8	..	..	..	..
4 0 2	8·2	6·8	5·7	6·6	7·3	6·6	6 0 1†	21·4	16·8	VVW	1·4	VVW	5·7
4 0 4	11·4	8·7	12·3	9·6	12·6	9·6	6 0 3	9·6	10·6	VVW	− 1·4	VVW	− 2·0
4 0 6	VVW	4·3	..	..	..	..	6 0 5	VVW	7·8	VVW	− 1·0	VVW	<1
4 0 8	VVW	2·0	..	..	..	..	6 0 7	6·0	6·6	..	..	..	..
6 0 2†	25·8	27·8	18·8	22·0	21·7	25·2	8 0 1	7·4	9·0	14·3	− 8·6	7·9	− 8·6
6 0 4†	12·1	4·8	4·2	− 3·0	5·7	− 3·6	8 0 3	4·8	7·3	10·6	7·7	5·7	7·7
6 0 6	VVW	∼0	..	..	..	..	8 0 5	5·2	7·4	..	..	..	..
6 0 8	6·7	13·0	..	..	..	..	8 0 7	2·8	5·2	..	..	..	..

† Reflexions whose signs could be determined by the method given in Section 5.

TABLE IV—(*Contd.*)

1	2	3	4	5	6	7	8	9	10	11	12	13	14
8 0 2†	25·4	29·0	19·7	21·2	22·2	25·1	10 0 1	VVW	− 8·1	..	..	..	..
8 0 4†	VVW	6·0	2·5	6·0	VVW	5·4	10 0 3	6·3	8·7	..	..	..	..
8 0 6	24·8	23·8	..	..	..	..							
							1 0 2†	50·3	−44·9	35·2	−40·8	43·9	−42·5
10 0 2	6·4	6·5	..	..	..	..	1 0 4†	25·2	25·1	17·6	18·5	21·8	21·2
10 0 4	7·2	7·2	..	..	..	..	1 0 6†	3·9	− 8·9	VVW	− 5·4	4·5	− 7·3
							1 0 8	12·0	−15·3	..	..	18·4	−14·9
1 0 1†	32·9	−25·5	27·3	−20·2	28·4	−22·8							
1 0 3†	5·9	1·5	15·7	−12·7	10·7	− 7·0	3 0 2†	25·0	19·5	25·8	29·2	26·1	24·5
1 0 5†	16·4	−13·0	VVW	− 1·7	9·8	− 7·5	3 0 4†	28·8	19·6	3·5	7·0	15·8	13·0
1 0 7†	15·1	18·0	6·3	10·9	11·0	13·5	3 0 6†	19·1	−21·1	8·4	−13·9	13·7	−18·3
1 0 9	3·0	1·0	..	..	..	..	3 0 8	4·9	8·3	..	..	..	..
3 0 1†	13·8	−12·2	3·3	− 9·8	6·3	−10·7	5 0 2	VVW	~ 0	VVW	− 1·8	VVW	2·5
3 0 3†	70·3	64·5	53·7	59·9	59·8	62·0	5 0 4†	24·4	20·4	4·2	8·4	15·6	13·7
3 0 5†	23·2	−18·6	17·3	−14·6	19·3	−16·9	5 0 6†	16·5	−16·4	..	..	..	..
3 0 7†	5·6	− 8·2	11·8	−10·6	6·2	− 9·9							
3 0 9	10·0	8·1	..	..	..	..	7 0 2†	40·4	−45·4	31·7	−42·3	35·3	−43·9
							7 0 4†	24·7	24·5	21·8	18·8	24·7	19·7
5 0 1†	15·9	14·5	9·9	12·6	11·5	13·2	7 0 6	VVW	− 5·9	..	..	..	..
5 0 3†	40·9	−34·0	33·6	−29·7	36·3	−31·8							
5 0 5	VVW	~0	..	..	VVW	− 1·6	9 0 2	8·8	9·4	10·0	6·0	9·4	6·9
5 0 7	6·0	6·9	..	..	8·5	9·3	9 0 4	8·5	7·6	..	..	..	..
							9 0 6	VVW	1·6	..	..	..	..
7 0 1†	9·6	6·7	..	..	3·5	4·7							
7 0 3†	11·9	−11·5	..	..	4·7	− 8·0	11 0 2	7·8	7·3	..	..	..	..
7 0 5†	12·5	11·2	..	..	10·0	6·1							
7 0 7	9·6	− 8·8	..	..	..	..							

† Reflexions whose signs could be determined by the method given in Section 5.

TABLE V

Observed and calculated structure factors, for the (hko) reflexions of $KMnO_4$ for CuK_α radiation

h k o	F_0	F_c	*h k o*	F_0	F_c
2 0 0	41·5	34·7	8 2 0	28·9	38·4
4 0 0	43·5	− 38·4	8 4 0	18·8	31·0
6 0 0	24·9	− 23·7			
8 0 0	53·8	− 56·1	2 1 0	89·3	100·3
10 0 0	VVW	~0	2 3 0	36·4	− 41·8
			2 5 0	21·1	38·3
0 2 0	112·3	−124·9			
0 4 0	82·0	94·5	4 1 0	11·2	− 5·8
0 6 0	30·2	− 37·8	4 3 0	10·3	18·1
			4 5 0	7·7	5·1
2 2 0	14·3	8·5			
2 4 0	16·0	9·8	6 1 0	55·5	52·6
2 6 0	VVW	− 1·9	6 3 0	30·8	− 37·4
			6 5 0	13·1	21·7
4 2 0	4·0	5·4			
4 4 0	10·0	− 12·8	8 1 0	7·4	10·4
4 6 0	2·0	3·7	8 3 0	9·5	− 13·8
6 2 0	11·0	− 12·6	10 1 0	23·6	− 24·3
6 4 0	9·6	− 7·2	10 3 0	18·8	15·4

TABLE VI

Discrepancy factor for $KMnO_4$ for (hol) reflexions

	CuKα	FeKα	CoKα
$\Sigma \lvert F_0 \rvert$ ..	1623·5	1016·7	1180·7
Taking all reflexions			
$\Sigma \lvert \lvert F_0 \rvert - \lvert F_c \rvert \rvert$ ..	275·9	167·0	174·0
R ..	0·170	0·164	0·147
Omitting unobservable reflexions			
$\Sigma \lvert \lvert F_0 \rvert - \lvert F_c \rvert \rvert$ ..	234·6	159·7	156·8
R ..	0·145	0·157	0·133

There is no doubt that theoretically at least the method of anomalous dispersion is capable of varied application. The method of using a wavelength longer than that of the absorption edge can be used for the determina-

tion of both centrosymmetric and non-centrosymmetric structures (not, however, the absolute configuration). When, on the other hand, a wavelength smaller than that of the absorption edge is used, the structure of both centro and non-centrosymmetric crystals can again be determined but with one significant difference, that the structure obtained in the non-centrosymmetric case would be the absolute configuration.

The determination of the signs of the structure factors of centrosymmetric crystals by the anomalous dispersion method seems to be very promising. But it is rather difficult to evaluate at this stage the power of this method. Whether this method would remain just a novelty or whether it would be capable of yielding practical results of significance is yet to be seen. One thing, however, is certain: that if any advance in this direction is to be made one has to abandon the photographic technique in favour of the very much more accurate Geiger or scintillation counter method of measuring intensities.

SUMMARY

The decrease in the scattering factor when the incident radiation is close to the absorption edge of an atom has been utilized for determining the structure of the centrosymmetric crystal $KMnO_4$. Multiple film zero-layer Weissenberg photographs were taken with CuK_α, CoK_α and FeK_α radiations, all of which are quite close to the K-absorption edge of the Mn atom. After reducing these data to the same relative scale, an Anomalous Difference Patterson (A.D.P.) map was computed with $(|F_{Cu}|^2 - |F_{Fe}|^2)$ as coefficient and it was found to have striking resemblance to the Isomorphous Difference Patterson map made with $(|F_{Cu}^{KMnO_4}|^2 - |F_{Cu}^{KClO_4}|^2)$ as coefficient. The structure was recovered from the A.D.P. diagram by means of the Buerger Vector shift method. An interesting offshoot of this technique is that the position of the excited atom could be directly determined by making a Patterson with $(|F_{Cu}| - |F_{Fe}|)^2$ as coefficient. From the knowledge of the position of the anomalously scattering atom and also its scattering factors for the different radiations, it was possible to assign the signs of as many as 50% of the reflexions. Commencing with these the structure was determined and the atomic parameters were refined. The final R-factor for the (*hol*) and (*hko*) projections were respectively 0·145 and 0·153. The parameters found are appreciably different from those reported earlier.

REFERENCES

1. Bijvoet, J. M. .. *Nature*, 1954, **173**, 888.
2. Booth, A. D. .. *Fourier Technique in Organic Structure Analysis*, Cambridge University Press, 1948.

3. Bradley, A. J. and Rodgers, J. W. — *Proc. Roy. Soc.*, 1934, **144 A**, 340.
4. Buerger, M. J. .. *Proc. Nat. Acad. Sci.*, 1942, **28**, 281.
5. ———— .. *Acta Cryst.*, 1951, **4**, 531.
6. Frueh, A. J. .. *Ibid.*, 1953, **6**, 454.
7. Harker, D. .. *Ibid.*, 1956, **9**, 1.
8. James, R. W. .. *The Crystalline State*, **II**, London, Bell, 1948.
9. Jones, F. W. and Sykes, C. — *Proc. Roy. Soc.*, 1937, **161 A**, 440.
10. Kartha, G. and Ramachandran, G. N. — *Acta Cryst.*, 1955, **8**, 195.
11. Mooney, R. C. L. .. *Phys. Rev.*, 1931, **37**, 1306.
12. Okaya, Y., Saito, Y. and Pepinsky, R. — *Ibid.*, 1955, **98**, 1857.
13. Ramachandran, G. N. and Raman, S. — *Curr. Sci.*, 1956, **25**, 349.
14. Wyckoff, R. W. G. .. *The Structure of Crystals*, Reinhold, 1935.

STUDIES ON THE NATURE OF THE RACEMIC MODIFICATIONS OF OPTICALLY ACTIVE COMPOUNDS IN THE SOLID STATE

Part XIII. Camphor-β-sulphonyl *o*-, *m*- and *p*-nitro phenylamides (*d*- and *dl*-), camphor-β-sulphonyl *o*-, *m*- and *p*-phenylene diamines (*d*- and *dl*-) and *o*-, *m*- and *p*-phenylene-*bis*-camphor-β-sulphonylamides (*d*- and *dl*-)

By Bawa Kartar Singh, F.A.Sc. and Shiva Mohan Verma

(Organic Chemistry Research Section, Banaras Hindu University, Banaras)

Received May 1, 1957

In this communication, which is in continuation of our previous work,[1] we describe the investigation of the nature of the racemic modifications of camphor-β-sulphonyl-nitro phenylamides (*o*, *m*- and *p*-), camphor β-sulphonyl-phenylene diamines (*o*-, *m*- and *p*-) and phenylene-*bis*-camphor-β-sulphonylamides (*o*-, *m*- and *p*-). Out of the three methods described previously by us,[2, 3, 4] the one based on Roozeboom's freezing point (melting point)-composition diagrams has been employed to diagnose the nature of the racemic modification. If the diagram is composed of (i) three curves, it is a true *dl*-compound, (ii) two curves, it is a mechanical mixture or *conglomerate* and (iii) one curve, a solid solution of the optically active and opposite forms. We have characterised five of the compounds as true *dl*-compounds and the remaining four as solid solutions, whereas no case of a mechanical mixture has been observed. As the diagrams are symmetrical, only one of the active forms is required for the study.

Experimental

The preparation and the purification of the compounds have been described already.[5] The melting point-composition diagrams (Figs. 1–8) were prepared as given in our previous paper.[1] Tables giving melting points and percentage compositions have been omitted to economise space.

Discussion

1. *Camphor-β-sulphonyl*-p-, m- *and* o-*nitrophenylamides*.—The melting point-composition diagram (Fig. 1 A) of the *para*-isomers consists of a single continuous curve with a maximum, which shows that the racemic form is a solid solution of the optically active and opposite forms. The melting point of the racemic form falls rapidly with the admixture of the *d*-form up to 50 per cent. and further admixture with *d*-form 60–100 per cent. hardly lowers

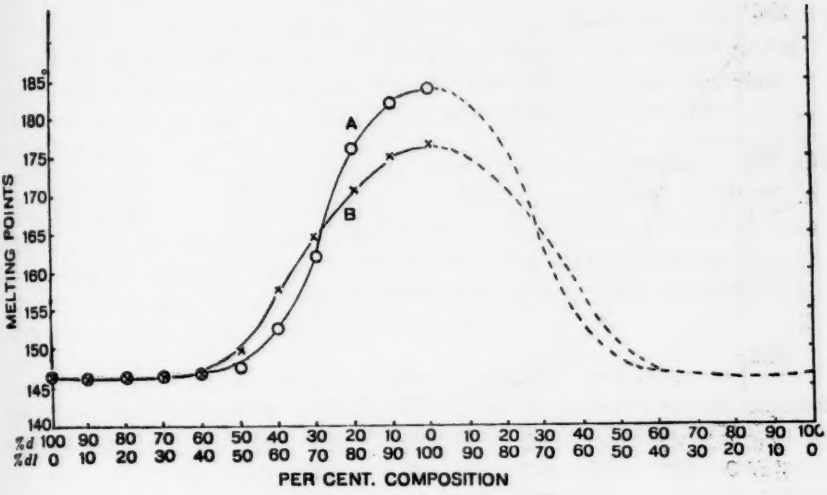

FIG. 1. A. Camphor-β-sulphonyl-*p*-nitro phenylamides O—O.
B. Camphor-β-sulphonyl-*m*-nitro phenylamides X—X.

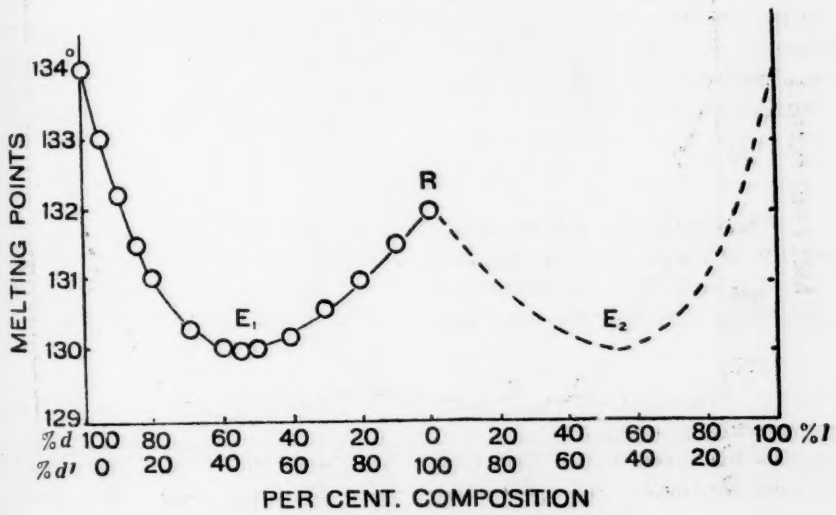

FIG. 2. Camphor-β-sulphonyl-*o*-nitro phenylamides.

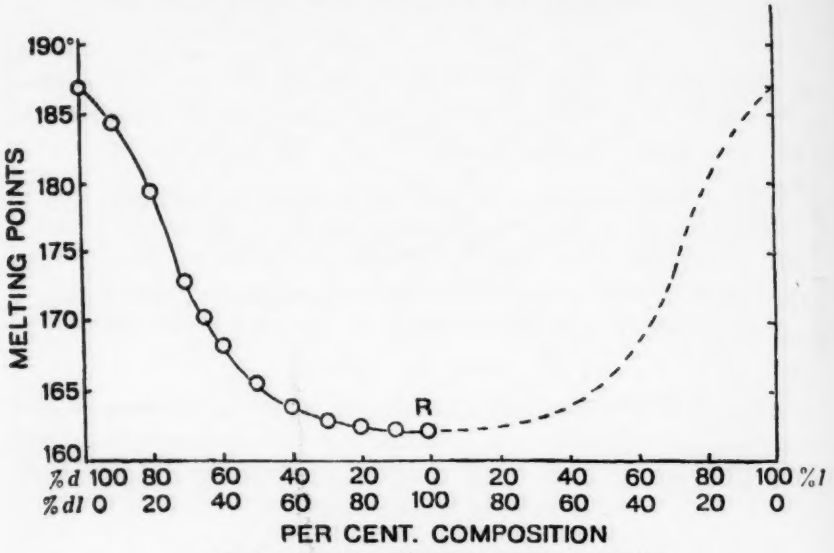

FIG. 3. Camphor-β-sulphonyl-*p*-phenylene diamines.

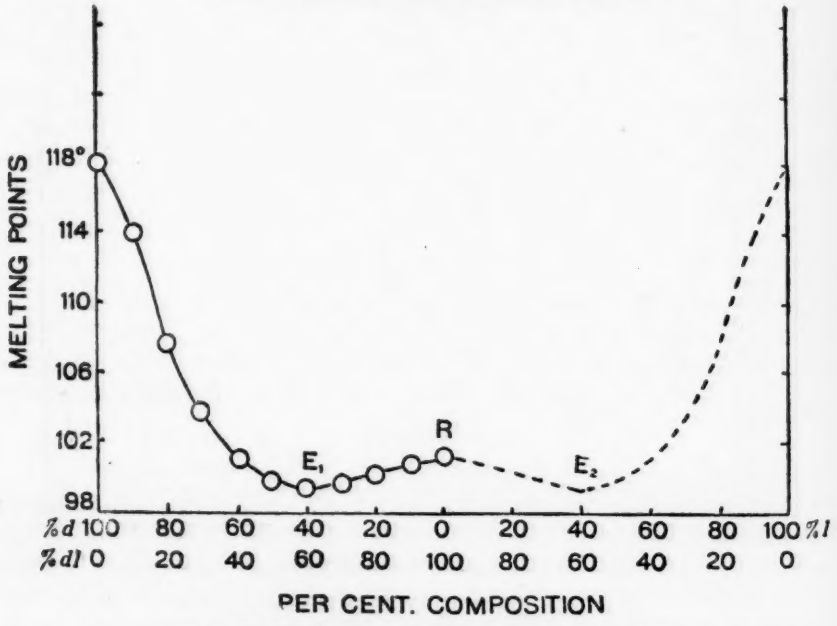

FIG. 4. Camphor-β-sulphonyl-*m*-phenylene diamines.

the melting point. The diagram (Fig. 1 B) of the *meta*-derivatives is very similar to that of the *para*-isomerides, consisting of only one continuous curve, which indicates the racemic form to be a solid solution. The melting point-composition diagram (Fig. 2) of *o*-isomerides consists of three curves with a central maximum R, which shows that the racemic form is a true *dl*-compound: *dl* - *d* and *dl* - *l* curves are fairly steep indicating that the racemic compound is stable and does not dissociate appreciably at its melting point. The central portion of the diagram does not occupy a large area, indicating its range of existence to be small. The eutectic points E_1 and E_2 are not sharp and well defined, indicating that in this region the active form and the racemic compound form solid solution.

2. *Camphor-β-sulphonyl*-p-, m- *and* o-*phenylenediamines.*—In the case of *meta* (Fig. 4) and *ortho* (Fig. 5) isomerides, the diagrams consist of three curves with a central maximum indicating the racemic forms to be *dl*-com-

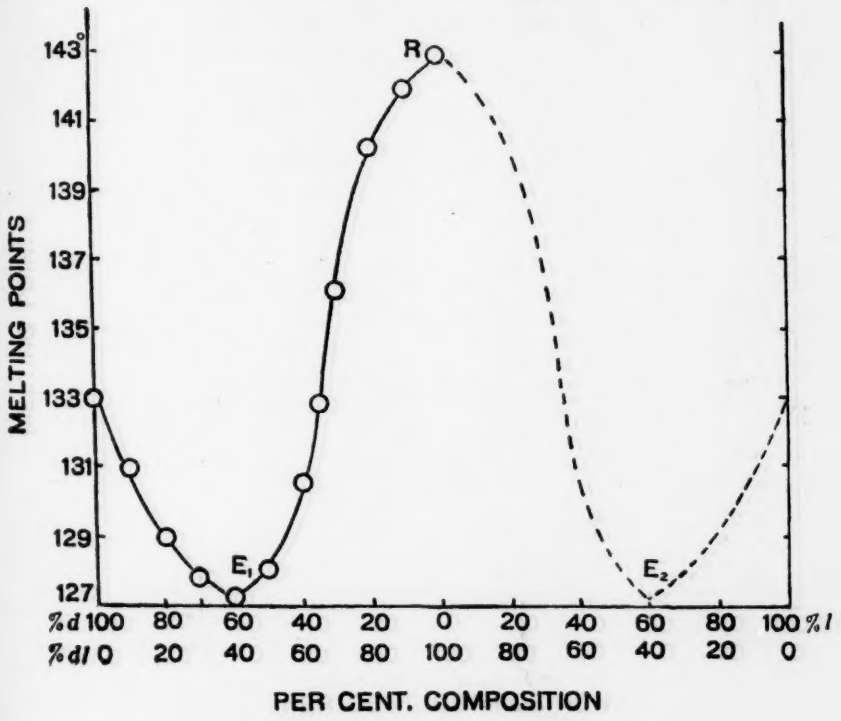

Fig. 5. Camphor-β-sulphonyl-*o*-phenylene diamines.

pounds. The central portion of the diagram for *m*-isomeride (Fig. 4) occupies a very small area and the eutectic points E_1 and E_2 are not sharp, indicating the low range of stability of the racemic form. On the other hand the central portion of the diagram in the case of the *o*-isomeride (Fig. 5) occupies a large area and the eutectic points are also well defined. This shows that the racemic form of the *o*-isomeride is more stable than that of the *meta*-isomeride. The steep fall of the curves, RE_1 and RE_2 (Fig. 5), indicates that the *ortho*-isomeride does not dissociate at its melting point. The melting point-composition diagram of the *para*-form (Fig. 3) has a minimum and the curve DRL, is continuous without any singular point, indicating the racemic form to be a solid solution.

3. p-, m- *and* o-*phenylene*-bis-*camphor*-β-*sulphonyl-amides*.—The melting point-composition diagrams of the *para* (Fig. 6) and *meta* (Fig. 7) iso-

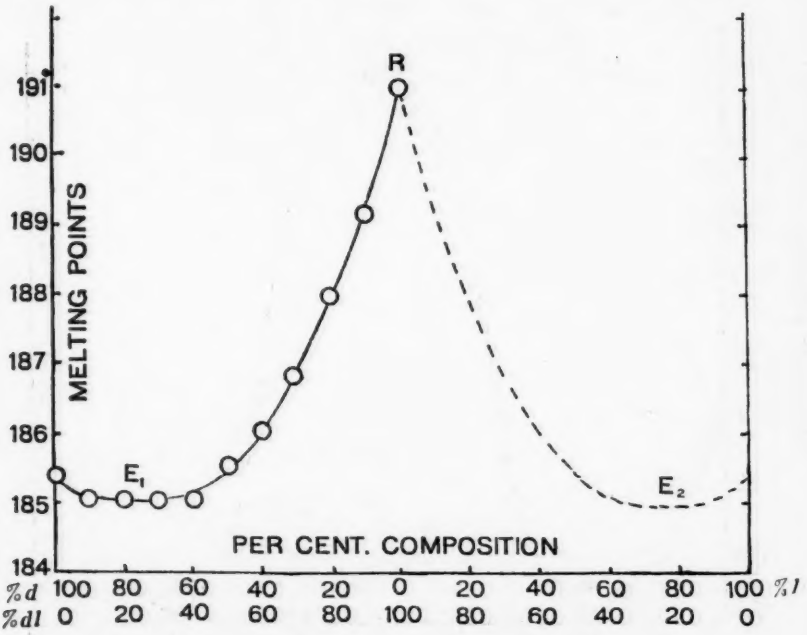

FIG. 6. *p*-phenylene-*bis*-camphor-β-sulphonyl amides.

merides show a central maximum and two eutectic points (E_1 and E_2). Each of them is composed of three curves DE_1, E_1RE_2 and E_2L, indicating the race-

mic forms to be true *dl*-compounds. In the case of *para*-isomerides (Fig. 6), the eutectic points are not sharp and well defined and the horizontal portion of the curve shows that the racemic compound forms solid solution with the *d*-form in the range between 90 per cent. *d*- to 60 per cent. *d*-isomerides. The steep curve, RE_1 shows that the racemic form is fairly stable. The diagram for the *meta*-isomerides (Fig. 7) has very sharp and well defined eutectic points; the curve, RE_1, is very steep, which indicates that the racemic compound is

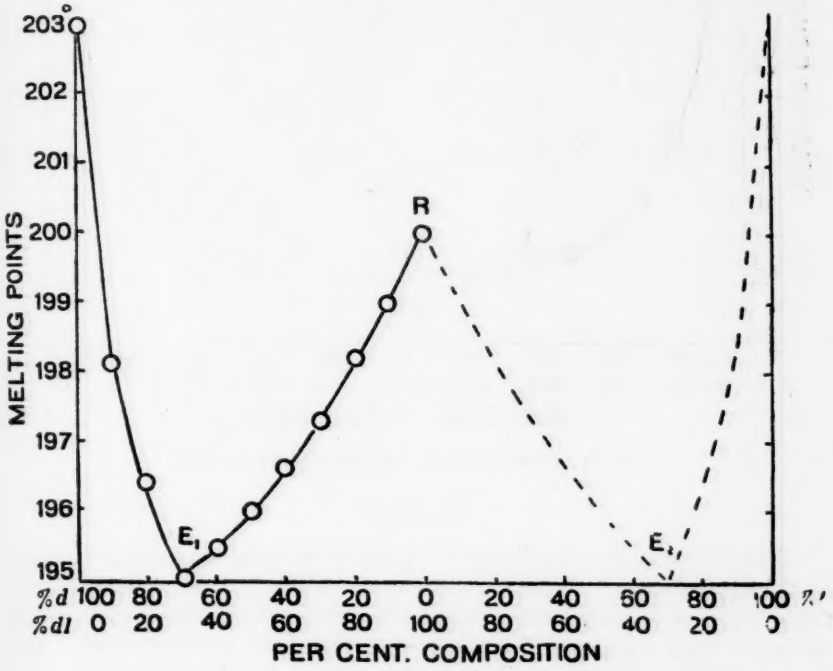

FIG. 7. *m*-phenylene-*bis*-camphor-β-sulphonyl amides.

very stable and does not dissociate at its melting point. Unlike *m*- and *p*-isomerides, the racemic form of the *o*-isomeride (Fig. 8) is a solid solution, which is evident from the continuous curve DE_1 RE_2L with a minimum. This curve is very similar to those obtained for *o*-chlorophenylimino and amino camphors[6] as well as camphor-β-sulphonyl-*p*-phenylenediamines described in this paper (Fig. 3).

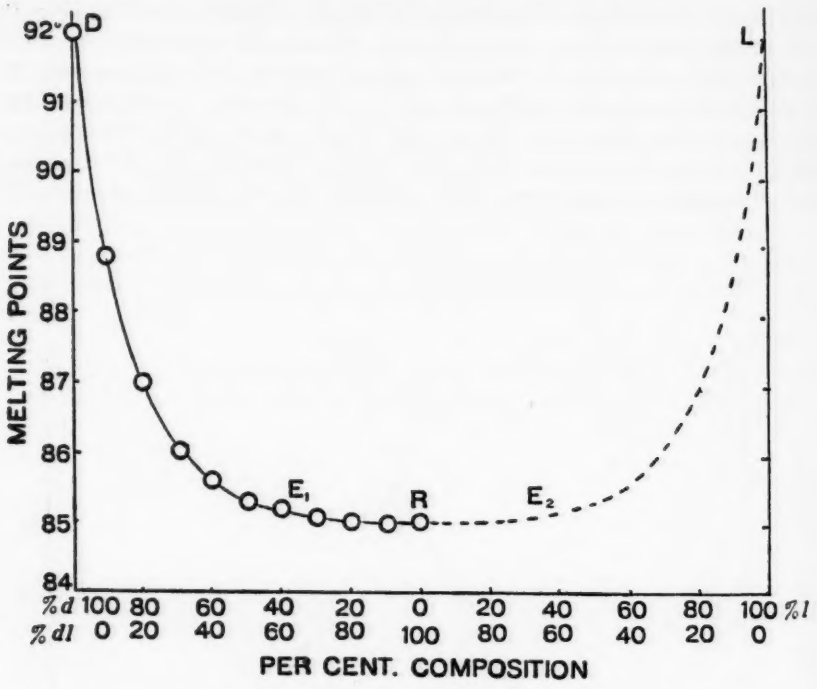

FIG. 8. *o*-phenylene-*bis*-camphor-β-sulphonyl amides.

SUMMARY

The nature of the racemic forms of the compounds has been investigated by the application of the melting point-composition method of Roozeboom. Out of the nine racemic forms, five have been found to be true *dl*-compounds varying in their stability and the remaining four form solid solutions. Two of the solid solutions, camphor-β-sulphonyl-*m*- and *p*-nitro-phenylamides give continuous curves with a maximum, while the remaining two, camphor-β-sulphonyl-*p*-phenylenediamines and *o*-phenylene-*bis*-camphor-β-sulphonyl-amides give continuous curves with a minimum.

ACKNOWLEDGEMENTS

We make grateful acknowledgements to the Banaras Hindu University for the provision of research facilities and to the Government of India, Ministry of Education, for the award of a Senior Research Scholarship to one of us (S. M. Verma).

REFERENCES

1. Singh, B. K. *et al.* .. *Proc. Ind. Acad. Sci.*, 1956, **43 A**, 44.
2. Roozeboom, B. .. *Ber.*, 1899, **32**, 537; *Z. Physikal Chem.*, 1899, **28**, 494.
3. Bruni .. *Gazzetta*, 1900, **30**, 35.
4. Singh, B. K. *et al.* .. *Proc. Nat. Acad. Sci., India*, 1944, **14**, 171.
5. ——— and Verma, S. M. .. *Proc. Ind. Acad. Sci.*, 1957, **45 A**, 298.
6. ——— and Seth, (Miss) S. K. *Jour. Ind. Chem. Soc.*, 1956, **33**, 491.

INFLUENCE OF CHEMISORBED CARBON MONOXIDE ON SUBSEQUENT PHYSICAL ADSORPTION OF NITROGEN

By V. Srinivasan

(Department of General Chemistry, Indian Institute of Science, Bangalore)

Received May 25, 1957

(Communicated by Prof. K. R. Krishnaswami, F.A.SC.)

Introduction

From studies[1, 2] on adsorption of CO and N_2 at low temperatures for estimating the free metal atoms on the surface of supported and promoted catalysts containing iron, cobalt or nickel, Anderson *et al.*,[1] and Emmett and Brunauer[2] concluded that (i) CO is first chemisorbed only on the metal surface after which it is physically adsorbed over the entire surface and (ii) the bare non-metallic surface and the chemisorbed film have the same adsorption characteristics. It is further assumed by Emmett and Brunauer, in the case of an iron catalyst, that CO chemisorbed at $-183°$ is not removed by evacuation at $-78°$ whereas all the physically adsorbed gas is desorbed at that temperature. They also observed that if an iron catalyst which had adsorbed CO at $-183°$ was evacuated at $-78°$ and then subjected to CO adsorption at $-183°$, the readsorption isotherm of CO coincided with the adsorption isotherm of N_2 at $-183°$ on the clean surface of the catalyst. They therefore suggested that the difference between the total adsorption of CO at $-183°$ on the clean surface and the readsorption value after evacuation at $-78°$ represented the extent of chemisorption of CO at $-183°$. Anderson *et al.*[1] on the other hand avoided this postulate of Emmett and Brunauer by assuming on theoretical grounds that the physical adsorption of CO should be equal to that of nitrogen and consequently the difference between the total CO adsorption and the nitrogen adsorption at the same relative pressure and low temperature represented the chemisorption of CO.

Joy and Dorling's[3] observation that a layer of chemisorbed CO on an iron catalyst does not suppress the subsequent adsorption of N_2 at $-195°$ supports the assumption of Emmett and Brunauer that the chemisorbed layer has the same adsorption characteristics as the rest of the surface.

As against the above, Stone and Tiley[4] who worked with a copper oxide catalyst noticed the suppression of physical adsorption of nitrogen and krypton at $-183°$ in the presence of chemisorbed CO and a similar observa-

tion in the case of three Fischer-Tropsch catalysts has been reported by Sastri and Srinivasan.[5] These observations invalidate the view that the chemisorbed layer and the bare surface have the same adsorption characteristics. The suppression of nitrogen adsorption in presence of chemisorbed CO clearly indicates that the chemisorbed CO layer restricts the adsorption of N_2 on the surface.

In view of the above discrepancies regarding an important aspect of adsorption processes and the non-validity of the assumption of Emmett and Brunauer, a revision of the method of estimating CO chemisorption seems to be called for. Experiments have therefore been conducted with a pure metallic surface (cobalt powder) thereby eliminating the interference of the non-metallic surface present in the case of experiments conducted by other workers. Reliable technique has been employed to investigate the influence of CO chemisorption on physical adsorption of nitrogen at −191°. Experiments carried out with sintered (500° C.) cobalt powder have thrown further light on the suppression effect.

Experimental

Cobalt powder.—Pure cobalt nitrate was decomposed to cobalt oxide at 300° C. 20·5 gm. of the oxide was reduced to the metal, in a glass catalyst tube having stopcocks at both ends (as shown in Fig. 1) by passing pure hydrogen at 300° C. for 96 hours to ensure complete reduction. Completion of reduction was ensured by sensitive tests on the exit hydrogen gas for absence of water vapour. The catalyst tube was then joined to the adsorption apparatus through stopcock S_2 as shown in Fig. 1.

Gases.—Helium for dead space measurements was obtained from a sealed helium tube containing helium of 99·9% purity imported from U.S.A. The gas was further purified by passing through activated charcoal cooled in liquid air.

Hydrogen for reduction was obtained by the electrolysis of 20% caustic potash solution and purified by passing through hot platinised asbestos to remove any oxygen present and dried by magnesium perchlorate and phosphorus pentoxide.

Carbon monoxide was prepared by the dehydration of formic acid by phosphoric acid at 180° C. The gas was purified by passing through caustic potash solution and caustic potash pellets to remove any CO_2 present and dried by passing through magnesium perchlorate and finally over phosphorus pentoxide. It was stored in gas jars over mercury.

Nitrogen from the cylinder was purified by passing through copper heated to 300° C. to remove any oxygen present and then dried by magnesium perchlorate and phosphorus pentoxide. It was stored in gas jars over mercury.

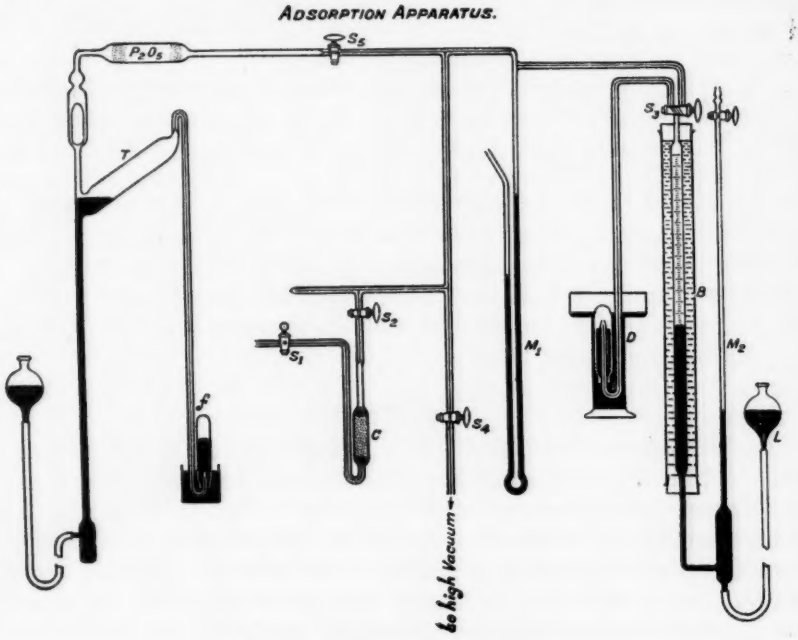

FIG. 1. Adsorption Apparatus.

Apparatus.—The adsorption apparatus used for this work is shown diagrammatically in Fig. 1. It consists of the catalyst tube C carrying stopcocks (S_1, S_2) at both ends and connected through tap S_2 to a mercury manometer M_1. The manometer is connected through a 3-way stopcock S_3 to a 50 c.c. burette graduated in tenths of a c.c. The burette which is enclosed in a water jacket W with a thermometer, is connected to a manometer M_2 for adjusting the pressure inside the burette by means of a mercury levelling bulb L supported on a movable ring. A screw adjuster attached to the ring is used for making fine adjustments. A travelling microscope with a scale micrometer eyepiece was used for reading the volume of the gas in the burette correct to 0·005 c.c. Stopcock S_3 is connected to a gas intake tube D dipping in a mercury reservoir for admission of gas into the apparatus. Stopcock S_4 connects the apparatus to an evacuation system consisting of a Leybold's

oil diffusion pump backed by a Cenco hyvac pump and an ultimate pressure of 10^{-5} mm. of Hg. as measured on a McLeod gauge attached to the system was obtained. The whole apparatus is connected to a Töpler pump T through stopcock S_5 for exhaustive desorption of the gas from the adsorbent and collection of the gas present in the apparatus. A thumb tube full of mercury was inverted over the fall tube of the Töpler (as shown in Fig. 1) for collection of the gas. The collected gas was transferred to the burette attached to the adsorption apparatus and measured.

Measurement of adsorption.—The dead space in the apparatus bounded by stopcocks S_2, S_4, S_5 and S_3 was measured by admitting consecutively, known volumes of a gas from the burette into the apparatus through S_3 and noting the pressure on the manometer M_1 and the atmospheric temperature. A calibration chart was made showing the volume of gas added against the closed limb reading of the manometer. The dead space in the catalyst tube at any temperature was determined by adding known volumes of helium into the adsorption system keeping the catalyst tube at the desired temperature and noting the pressure on M_1. As the dead space in the system up to tap S_2 corresponding to any closed limb reading is known from the previous chart, the dead space in the catalyst tube could be calculated at any pressure. A chart of catalyst tube dead space *versus* the pressure was drawn for the desired temperatures.

Adsorption measurements were carried out by first evacuating the adsorbent for 8 hours at 300° C. and then maintaining the adsorbent at the desired temperature while admitting known volumes of the adsorbable gas from the burette. As the dead space in the catalyst tube and the rest of the system are known, the extent of adsorption could be calculated for any temperature and pressure.

Temperatures for adsorption measurements.—Liquid air in Dewar Flasks was used for maintaining a temperature of −191°. Other temperatures were obtained by using solid CO_2-acetone (−78°), melting ice (0°), boiling acetone (53°) and boiling water (97°). An electric-furnace controlled by a Sunvic Energy Regulator to ±1° was used for maintaining temperatures of 200° C. and above for purposes of degassing, etc.

Adsorption experiments.—The following adsorption experiments were conducted on the sample of cobalt powder. Prior to each set of experiments the powder was soaked in hydrogen for 12 hours at 300° C. and then degassed for 8 hours at the same temperature. Three sets of experiments designated 1, 2 and 3 respectively were carried out. Each experiment involved 5 steps: (i) adsorption of nitrogen on clean surface at −191°, (ii) degassing at 10^{-5} mm.

for 8 hours at 300° C., (iii) adsorption of CO at −191° on the clean surface, (iv) exhaustive desorption of CO at the required temperature by means of the Töpler (at the highest pressure of adsorption) and collection and measurement of the desorbed gas (and the gas in the system bounded by S_1, S_4, S_5 and S_3). Calculation of the volume of undesorbed gas, *i.e.*, the gas retained on the surface, (v) subsequent adsorption of N_2 at −191° by the surface having undesorbed CO. The only variation in the three experiments was the temperature of desorption, *viz.*, step (iv), this being 0° in 1, 53° in 2, and 97° in 3.

After completing experiments 1–3, the cobalt powder was heated to 325° C. and degassed for 8 hours for experiments 4 and 5, which were conducted in the same manner as 1 except that the desorption temperatures were 0° and 97° respectively.

Experiments 6 and 7 were similarly performed on the same sample but heated to 370° C. and 500° C. respectively the desorption temperature being 0° C. in both the cases.

The above-noted experimental procedure for ascertaining the volume of CO retained on the surface of the catalyst is more direct and simpler than that adopted by previous workers. Joy and Dorling, for instance, desorbed the adsorbed CO by means of a diffusion pump at −78° and then readsorbed CO at −195°. The difference between the original and the readsorption values for CO was taken to represent the volume of CO retained on the surface of the catalyst. In the present case the modification of the experimental technique by the use of a Töpler pump for desorption and collection and subsequent measurement of the gas in the system has the following advantages: (i) The difference between the total volume of CO added to the system at the highest pressure of adsorption and the volume of CO taken out through the Töpler gives a direct estimate of CO retained on the surface of the catalyst at any temperature. (ii) It avoids the determination of a readsorption isotherm of CO at −191°. (iii) It was further possible to ascertain the volumes of CO retained on the catalyst surface at different temperatures easily.

RESULTS AND DISCUSSION

The results obtained from the experiments 1–7 are presented in Table I and since the determinations were made at different relative pressures thereby rendering comparison difficult, they have also been plotted in Figs. 2, 3 and 4.

The results presented in Table I show clearly that the value for V_m (N_2) calculated by the B.E.T. method (Col. 9) as well as the CO chemisorp-

TABLE I

Chemisorption of CO on cobalt

Weight of cobalt powder taken = 15·03 g.

1	2	3	4	5	6	7	8	9
Expt. No.	Temp. of preparation °C.	p/p_0 before desorption	Desorption temp. °C.	CO added c.c.	CO desorbed c.c.	CO retained c.c.	CO chemisorbed (Anderson[1]) c.c.	V_m (N_2) B.E.T. c.c.
1	300	0·662	0	73·03	66·44	6·59	5·60	6·67
2	300	0·633	53	69·61	63·85	5·76	5·60	6·67
3	300	0·613	97	67·59	62·76	4·83	5·60	6·67
4	325	0·644	0	68·81	62·95	5·86	5·30	5·20
5	325	0·544	97	58·77	54·68	4·09	5·30	5·20
6	370	0·667	0	68·76	64·20	4·56	4·90	4·35
7	500	0·630	0	58·01	56·45	1·56	2·00	1·97

tion value reckoned by Anderson's method (Col. 8) remain constant during the first 3 experiments 1–3 (thereby establishing the reproducibility of the surface of the adsorbent) although the volumes of CO retained on the surface as ascertained directly were found to progressively diminish quite considerably with increasing temperature of desorption in the three experiments. Further, the surface area of the same adsorbent is seen to fall progressively when subjected to temperatures above 300° C. reaching finally at 500° C. about one-third of its original value thereby indicating profound changes. The results given in Col. 7 of the table (experiments 1–5) show that the quantity of CO retained on the surface of the adsorbent diminishes considerably with increasing temperature of desorption. This important feature of the desorption process seems to vitiate Joy and Dorling's attempt to differentiate between the weakly and strongly chemisorbed gas because their consideration is limited to a desorption temperature of −78°.

The data obtained concerning the suppression of nitrogen adsorption by the presence of chemisorbed CO on the surface of cobalt powder are given belew in Table II.

TABLE II

Suppression of adsorption of nitrogen on surface having chemisorbed carbon monoxide

Weight of cobalt powder = 15·03 g.

Expt. No.	p/p_0	CO adsorption c.c.	p/p_0	N_2 adsorption c.c.	p/p_0	N_2 adsorption on surface with chemisorbed CO c.c.
1	0·175	13·59	0·047	6·84	0·072	6·82
	0·299	14·65	0·176	8·07	0·198	7·79
	0·422	15·51	0·358	9·38	0·293	8·32
	0·542	16·35	0·429	9·81	0·401	9·10
2	0·117	13·05	0·148	7·78	0·166	7·43
	0·253	14·03	0·221	8·30	0·250	8·00
	0·377	15·00	0·308	9·18	0·337	8·60
	0·502	15·87	0·415	9·95	0·419	9·21
3	0·218	13·74	0·180	8·19	0·162	7·40
	0·354	14·82	0·261	8·74	0·208	7·85
	0·479	15·56	0·338	9·28	0·302	8·41
	0·613	16·43	0·419	9·82	0·402	9·11
4	0·137	11·82	0·223	6·82	0·171	6·26
	0·277	12·66	0·308	7·45	0·263	6·68
	0·421	13·10	0·387	7·90	0·338	7·14
	0·534	14·25	0·459	8·26	0·421	7·53
5	0·145	11·85	0·213	6·74	0·090	5·97
	0·278	12·50	0·307	7·51	0·199	6·45
	0·396	13·05	0·386	7·82	0·307	6·90
	0·544	13·93	0·461	8·17	0·420	7·42
6	0·125	9·77	0·177	5·51	0·165	5·23
	0·295	10·62	0·227	5·80	0·246	5·50
	0·419	11·44	0·308	6·12	0·338	6·08
	0·553	11·91	0·393	6·40	0·428	6·40
7	0·133	4·36	0·142	2·56	0·146	2·54
	0·213	4·59	0·197	2·59	0·234	2·75
	0·342	4·77	0·338	2·91	0·322	2·74
	0·489	5·11	0·425	2·99	0·429	2·89

The data presented above in Table II are not easy to compare and so have been plotted in the curves in Figs. 2, 3 and 4 respectively. The results of experiments 1, 2 and 3 are shown in curves A, B and C in Fig. 2. Curves

A and B which connect all the values for carbon monoxide adsorption and for nitrogen adsorption respectively on the clean surface obtained in the three experiments reveal clearly that the surface was perfectly reproducible under the experimental conditions adopted. Curve C represents the volumes of nitrogen adsorbed on the cobalt surface having different amounts

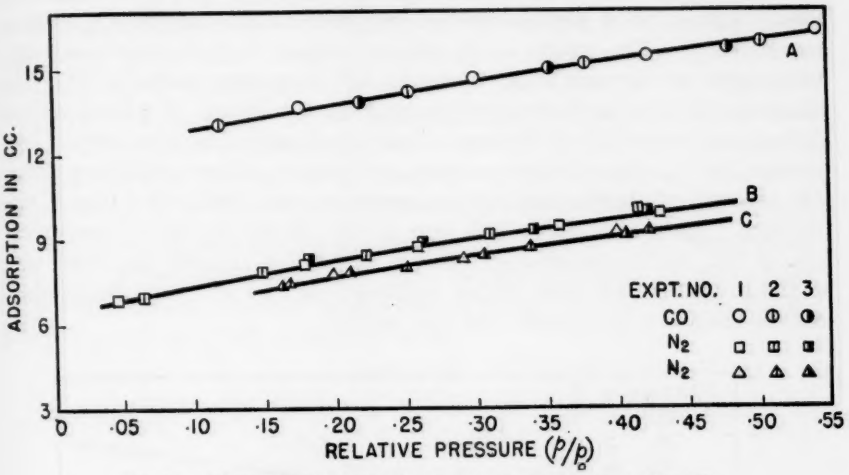

FIG. 2. Adsorption of CO and N_2 at −191° C. (Expt. Nos. 1, 2 and 3).

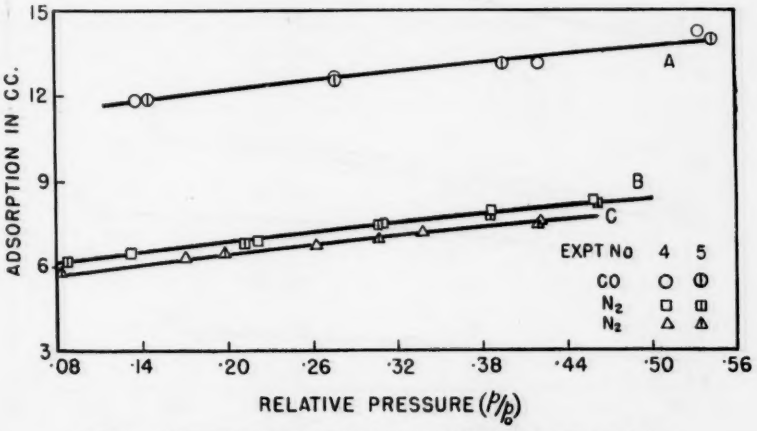

FIG. 3. Adsorption of CO and N_2 at −191° C. (Expt. Nos. 4 and 5).

of chemisorbed carbon monoxide, namely, 6·59, 5·76 and 4·83 c.c. respectively in the three experiments, this being due to the employment of different

desorption temperatures, *viz.*, 0°, 53° and 97° respectively. Curve C is seen to be parallel to curve B throughout the range of p/p_0 studied and the nitrogen adsorption values through the p/p_0 range studied, being 0·60 c.c. less than the values for the adsorption on the clean surface. This observation seems to establish that the suppression of the nitrogen adsorption on the surface of cobalt having chemisorbed carbon monoxide remains constant within the limits of variation of the chemisorbed carbon monoxide and the p/p_0 covered in this study. The results of experiments 4 and 5 which were conducted with cobalt powder previously heated to 325° have been plotted in Fig. 3 in which curves A and B represent respectively the values of adsorption of carbon monoxide and of nitrogen on the clean surface whereas curve C represents the nitrogen adsorption values on the same surface containing different amounts of chemisorbed carbon monoxide, *viz.*, 5·86 and 4·09 c.c. respectively. Here also, curve C is seen to run parallel to curve B indicating clearly that the suppression of nitrogen adsorption remains the same, *viz.*, 0·55 c.c. whether the cobalt surface contains 5·86 or 4·09 c.c. of chemisorbed carbon monoxide throughout the p/p_0 studied.

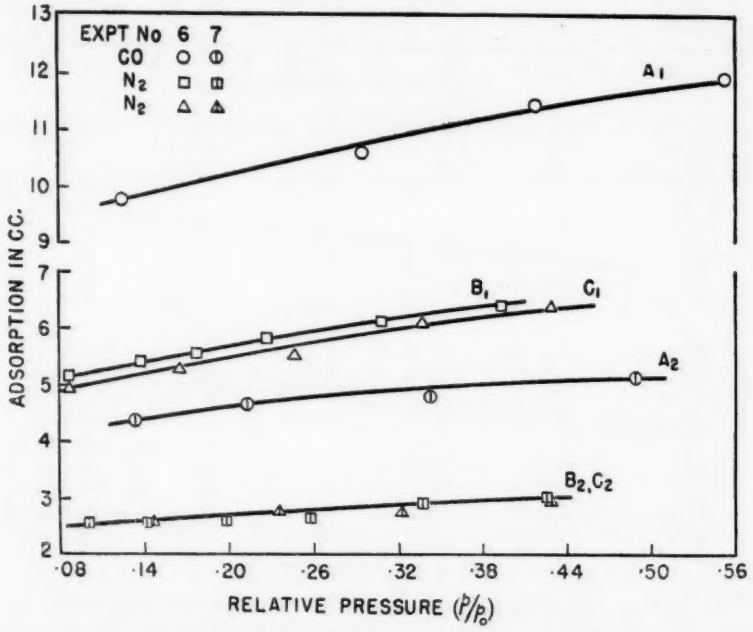

FIG. 4. Adsorption of CO and N_2 at −191° C. (Expt. Nos. 6 and 7).

The results of experiments 6 and 7 have been plotted in Fig. 4. The curves A_1 and B_1 represent respectively the adsorptions of carbon monoxide and of nitrogen on the clean surface of the cobalt powder which has been previously heated to 370° while curve C_1 represents the nitrogen adsorption on the same surface containing 4·56 c.c. of chemisorbed carbon monoxide. Here again it is seen that curve C_1 runs parallel to B_1 showing that in the range of conditions studied the adsorption of nitrogen is suppressed to the extent of 0·10 c.c. The curves A_2 and B_2 represent the adsorptions obtained when the cobalt powder had been heated at 500° prior to the experiment while curve C_2 represents the nitrogen adsorption on the same surface with 1·56 c.c. chemisorbed carbon monoxide. Curves C_2 and B_2 are practically identical showing that the nitrogen adsorption values were not affected by the presence of chemisorbed carbon monoxide on the surface of cobalt powder.

The above observations are summarised below in Table III, which shows the extent of the suppression of nitrogen adsorption at liquid air temperature on surfaces having different adsorptive capacities and containing varying amounts of chemisorbed carbon monoxide.

TABLE III

Adsorptions of CO and of N_2 at −191°, the desorptions being at 0°, 53° and 97°

Weight of Cobalt Powder = 15·03 g.

Expt. No.	Prepared at °C.	CO adsorption at p/p_0=0·4 (from isotherms) c.c.	CO undesorbed c.c.	Suppression of N_2 adsorption c.c.
1	300	15·30	6·59	0·60
2	300	15·30	5·76	0·60
3	300	15·30	4·83	0·60
4	325	13·40	5·86	0·55
5	325	13·40	4·09	0·55
6	370	11·30	4·56	0·10
7	500	5·00	1·56	0·00

It can be seen from Table III that the suppression of nitrogen adsorption is of the order of 0·60 c.c. in presence of 5·86 and 4·09 c.c. of carbon

monoxide even in the case of the powder heated to 325° C. although the total carbon monoxide and nitrogen adsorption at −191° C. and 0·4 relative pressure fall from 15·25 and 9·72 c.c. to 13·40 and 8·00 c.c. respectively (Table I, Figs. 2 and 3). Further in the case of the cobalt powder heated to 370°, the suppression of nitrogen adsorption in presence of 4·56 c.c. of carbon monoxide is only 0·10 c.c., the suppression effect completely disappearing in the case of the adsorbent heated to 500° C. Moreover, the decrease in suppression is not proportional to the decrease in surface areas as is seen from the V_m (N_2) values presented in Table I. Thus it is clear that the suppression effect is not a function of the surface area or of the volume of carbon monoxide present on the surface but mainly due to the surface heterogeneity of the cobalt powder. It may be assumed that although carbon monoxide is chemisorbed over the entire surface of the cobalt at −191°, there are some highly active centres on the surface of cobalt where the carbon monoxide chemisorption is of a different nature from that on the rest of the surface, and such strongly held carbon monoxide does not adsorb any nitrogen at −191°, whereas the rest of the surface with chemisorbed carbon monoxide allows physical adsorption thus having adsorption characteristics similar to a non-metallic surface. Such strong chemisorption seems to be equivalent to the suppression of nitrogen adsorption noticed in the various experiments namely to 0·60 c.c. of nitrogen adsorption.

When the cobalt powder is heated to 370°, the highly active centres are destroyed and carbon monoxide chemisorbed on the surface behaves like a bare surface for physical adsorption of nitrogen and only 0·10 c.c. suppresion of nitrogen adsorption is observed. On heating the adsorbent to 500° C., the cobalt surface undergoes a drastic change resulting in a large fall in surface area and in the total adsorptions of carbon monoxide and nitrogen and at the same time the centres responsible for 0·10 c.c. suppression of nitrogen adsorption also disappear.

The entire set of experiments were repeated with a smaller sample (6·6 g.) of cobalt powder and all the observations recorded above were fully confirmed. Limitations of space prevent the presentation of the results of these experiments.

The foregoing observations offer a clue to explain at the same time the contradictory observations of Stone and Tiley[4] and of Joy and Dorling[3] because both these have been observed in this work with cobalt powder. The cobalt powder heated to 300° C. shows suppression of nitrogen adsorption whereas after heating to 370° , there is no suppression of nitrogen adsorption in presence of chemisorbed carbon monoxide. As the preparation of

iron synthetic ammonia catalyst requires a high temperature, it would appear that certain sensitive centres responsible for the suppression effect are destroyed during the process of preparation and hence no suppression effect was observed by Joy and Dorling in the case of their iron catalyst.

These results also throw light on the determination of chemisorption of carbon monoxide on cobalt. Where there is no suppression of physical adsorption, Anderson's method of calculating chemisorbed carbon monoxide as the difference between the carbon monoxide adsorption and nitrogen adsorption, both on the clean surface at −191° would hold good. On the other hand, in the case of catalysts where there is suppression of physical adsorption of nitrogen in presence of chemisorbed carbon monoxide, the assumption of Emmett and Brunauer and of Anderson *et al.* that the entire chemisorbed surface has the same adsorption characteristics as the bare non-metallic surface would appear to be invalid. Thus even a pure metallic surface seems to consist of two parts, one where the chemisorbed layer of carbon monoxide allows physical adsorption of nitrogen and the other made up of certain active centres where subsequent adsorption of nitrogen does not take place. Thus in the case of supported catalysts where suppression of physical adsorption in presence of chemisorbed carbon monoxide has been observed, the suppression is not due to the non-homogeneity of the entire chemisorbing surface as metallic and non-metallic for physical adsorption but due to the carbon monoxide chemisorbed on active centres.

A method may now be suggested for determination of chemisorption. Anderson *et al.*[1] have postulated that the physical adsorption of carbon monoxide is equal to that of nitrogen and have therefore taken the difference between the total adsorption of carbon monoxide and the nitrogen adsorption on the clean surface at the same relative pressure and low temperature to be the carbon monoxide chemisorption. In cases where chemisorbed carbon monoxide suppresses the physical adsorption of nitrogen, it is clear that the chemisorbed carbon monoxide should suppress its own physical adsorption also. The suppressed physical adsorption isotherm of carbon monoxide can be considered to be identical with the suppressed nitrogen adsorption isotherm as these two gases have equal physical adsorptions. Hence the following procedure can be adopted for determining carbon monoxide chemisorption: (i) Determination of carbon monoxide chemisorption on clean surface at −191°. (ii) Exhaustive desorption of carbon monoxide at any convenient temperature ranging from 0–100° C. (iii) Adsorption of nitrogen at −191° on this surface. The difference between the total carbon monoxide adsorption isotherm and the nitrogen adsorption isotherm on the chemisorbed

surface would give a truer estimate of carbon monoxide chemisorption as it would eliminate the error due to suppression of physical adsorption effect.

Thus in the present case it can be seen from Fig. 2 that the difference between Curve A (total CO adsorption) and curve C amounting to 6·20 c.c. gives a truer estimate of carbon monoxide chemisorption as compared to the difference between curves A and B amounting to 5·60 c.c.

In the light of experience gained in studies[6] on chemisorption of carbon monoxide on nickel, where formation of nickel carbonyl was definitely established, similar attempts were made to ascertain if formation of any chemical compound of cobalt could be detected in the experiments described in this paper, but in no case and under no conditions could the removal of any cobalt atoms from the surface be detected.

SUMMARY AND CONCLUSION

1. The investigation of the effect of chemisorbed layer of carbon monoxide on subsequent adsorption of nitrogen at −191° on two samples of cobalt powder has shown that (*a*) the presence of a layer of chemisorbed carbon monoxide suppresses the nitrogen adsorption at −191°, (*b*) the suppression is constant irrespective of the volume of carbon monoxide on the surface, (*c*) the suppression effect disappears on heating the samples to 370° and above.

2. The suppression of nitrogen adsorption appears to be due to the presence of certain active centres on the surface of cobalt powder and which chemisorb carbon monoxide in such a manner that subsequent adsorption of nitrogen does not take place on such chemisorbed centres.

3. When suppression of nitrogen adsorption takes place in presence of chemisorbed carbon monoxide, the assumption of Emmett and Brunauer that the entire chemisorbed surface has the same adsorption characteristics as a bare non-metallic surface is invalid.

4. A method has been suggested for determination of carbon monoxide chemisorption in cases where suppression of nitrogen adsorption in presence of chemisorbed carbon monoxide is observed.

ACKNOWLEDGEMENT

The author wishes to place on record his profound sense of gratitude to Prof. K. R. Krishnaswami for his interest and guidance throughout this investigation. The author also wishes to thank the Government of India for the award of a Senior Research Scholarship which enabled him to complete this investigation.

References

1. Anderson *et al.* .. *J.A.C.S.*, 1948, **70**, 2465.
2. Emmett and Brunauer .. *Ibid.*, 1937, **59**, 310, 1553.
3. Joy and Dorling .. *Nature*, 1951, **168**, 433.
4. Stone and Tiley .. *Ibid.*, 1951, **167**, 654.
5. Sastri and Srinivasan .. *Curr. Sci.*, 1954, **23**, 154.
6. Srinivasan and Krishnaswami *Ibid.*, 1956, **25**, 328.

THE CRYSTAL STRUCTURE OF AMMONIUM PERCHLORATE—NH_4ClO_4

By K. Venkatesan

(*Department of Physics, Indian Institute of Science, Bangalore-3*)

Received May 10, 1957

(Communicated by Dr. R. S. Krishnan, F.A.Sc.)

1. Introduction

Although the crystal structures of NH_4ClO_4[1] and its isomorph $KMnO_4$[2] have been reported, Wyckoff[3] makes the following remarks in his book *The Structure of Crystals*—" These crystals have units which are almost identical in size and it is probable that their real atomic positions are practically the same. Nevertheless the structures proposed for the permanganate and for the perchlorates show important differences. The potassium permanganate determination rests on photographic spectral data; the observations on potassium perchlorate and ammonium perchlorate are more quantitative spectrometric measurements. It is, however, difficult to be sure of the deductions from the latter results. The published parameters are obviously wrong; they correspond to an impossible grouping." In view of the above remarks, a thorough and accurate study of these crystals has been undertaken. Recently, using the anomalous scattering technique, the structure of $KMnO_4$[4] has been determined to a fair degree of accuracy. The parameters deduced were considerably different from those reported by Mooney.[2] Ammonium perchlorate was next taken up for accurate study. One of the chief objects of the investigation was to determine the positions of the hydrogen atoms and also to find out whether the structure has any hydrogen bonds in it. The results obtained are presented in this paper.

2. Morphological and Optical Data

Ammonium perchlorate crystallizes in the form of needles elongated along the *b*-axis. From morphological studies the crystal is known to belong to the orthorhombic bipyramidal class with the axial ratios.

$$a : b : c = 0{\cdot}7932 : 1 : 1{\cdot}2808.$$

The *m* planes {110} and the *c* planes {001} are the most prominent. The crystal exhibits a weak positive birefringence, and its refractive indices are $\alpha = 1{\cdot}481$, $\beta = 1{\cdot}483$ and $\gamma = 1{\cdot}488$ and $2V = 68°$.

3. Unit Cell and Space-Group

The unit cell, as determined from Weissenberg photographs, is

$$a = 9{\cdot}13 \text{ Å} \qquad b = 5{\cdot}79 \text{ Å} \qquad c = 7{\cdot}47 \text{ Å}$$

The axial ratios are thus $1{\cdot}579 : 1 : 1{\cdot}290$. The ratios are in fair agreement with the morphological values given by Barker,[5] if one takes Barker's (*hkl*) as (2 *h*, *k*, *l*). The space-group is found to be *Pnma* in agreement with the results of the previous investigators. The density of the crystal is 1·952 and the number of molecules per unit cell is 4.

CuKα radiation and the multiple-film technique were employed in taking zero-layer Weissenberg photographs about the *b*- and *c*-axes. The relative intensities of the reflexions were estimated visually. The values were corrected for Lorentz and Polarization factors and the correction for absorption was made using Bradley's method for cylindrical specimens.

To obtain the correct distribution of the atoms among the available positions in the space-group *Pnma*, one could make use of the fact that ClO_4 and NH_4 ions are approximate tetrahedra. The asymmetric unit, therefore, consists of one nitrogen, one chlorine, four oxygens and four hydrogens. This leads one to the conclusion that the chlorine, the nitrogen, two hydrogens and two oxygens of the ClO_4 group must lie on the reflexion planes at $y = \pm{\cdot}25$ and the other two oxygen atoms of the ClO_4 group and the two hydrogen atoms of the NH_4 ion must be equidistant from the mirror plane, one being the mirror image of the other. Hence we find that the *y* parameter of all atoms except the two oxygen and two hydrogen atoms which occupy general positions should be $\pm b/4$.

4. The *b*-Axis Fourier Projection

When the Patterson projection on (010) was made it was found that due to lack of resolution of the peaks it was possible to get the approximate (*x*, *z*) co-ordinates of the chlorine and nitrogen atoms only. Consequently, the structure factors of ammonium perchlorate were calculated using the parameters of the corresponding atoms of the isomorph $KMnO_4$.[4] The parameters used are given in Table I.

The signs of about 30 strong reflexions out of the total of about 90 reflexions of the type (*hol*) could be determined unambiguously. These reflexions were used to compute the first Fourier synthesis using the relevant electron density expression[6] for the (010) projection for the space-group *Pnma*. The

Fourier summation was performed using the Beevers-Lipson strips at intervals of 6°. The atomic co-ordinates were refined by the iterative process of

TABLE I

Atom	x	z
Cl (Mn)	0·438	0·192
N (K)	0·183	0·158
O_1	0·321	0·038
O_2	0·594	0·106
O_3	0·417	0·317
O_4	0·417	0·317

Fourier syntheses. At each stage of the refinement the scale and temperature factors were obtained from the graph plotted between $\log_e \Sigma|F_c|/\Sigma|F_o|$ and $\sin^2\theta$. After the final projection, Booth's back correction method was used to eliminate the errors due to the termination of the Fourier series and the magnitude of these errors were of the order of 0·06 Å. The discrepancy factor at this stage was 0·231.

5. DETERMINATION OF THE y CO-ORDINATE

As mentioned earlier, the space-group demands that all atoms except the two oxygen atoms of the ClO_4 group should lie on the mirror planes at $y = \pm 0{\cdot}25$. Since there were only 35 (*hko*) reflexions, the least squares method was considered to be more suitable than the Fourier method. The approximate y co-ordinate of the oxygen atoms O_3 and O_4 off the mirror plane was calculated as follows:—The projection of the Cl—$O_{(2)}$ distance on the (010) plane was found from the b-axis Fourier projection to be 0·817 Å. Assuming the angle of O_3ClO_4 to be the tetrahedral angle, the distance of the oxygen from the mirror plane was calculated to be 0·192 in fractional co-ordinate. The y co-ordinate was changed by trial so as to attain better agreement between the calculated and observed structure amplitudes for the (*oko*) reflexions. The value of y thus obtained was 0·050. The scale and temperature factors were respectively 1·6 and $2{\cdot}7\times10^{-16}$. The discrepancy factor was as low as 0·131. In evaluating the discrepancy factors given in this paper a few reflexions with very weak intensities have been omitted,

6. Refinement of Atomic Parameters

The approximate y parameter of the oxygen atom in the general position was refined by the method of least squares.[7] Neglecting, to a first approximation, the off-diagonal terms of the normal equations, we get

$$\Delta y_n \sum w \left(\frac{\partial F_c}{\partial y_n}\right)^2 = \sum w (F_o - F_c) \frac{\partial F_c}{\partial y_n} \qquad (1)$$

where w the weight to be given to each reflexion was taken to be equal to unity. Such of those reflexions which are believed to have been affected by extinction were given zero weight. Three cycles of the least squares treatment gave $y = 0{\cdot}044$, the next cycle giving a negligible value for Δy. The final discrepancy factor for this zone came out of the order of $0{\cdot}128$.

The (xz) co-ordinates were further refined by a succession of $(F_o - F_c)$ syntheses. These indicated slight movements of the oxygen atoms and also that the temperature factor on the oxygens had to be increased. When these changes were made it was noticed that the calculated amplitudes were very much higher than the observed ones in some of the strongest reflexions. The values for I_c/I_o plotted against I_c for these reflexions lay very nearly on a straight line. When the effect of extinction was taken into account the value of the discrepancy factor came out to be $0{\cdot}151$.

7. Hydrogen Positions

A further difference projection with reflexions affected by extinction removed was prepared and it was found from it that the nitrogen was surrounded by three electron density maxima, giving an indication of the probable hydrogen positions. In fact one can discern the positions of two hydrogens even in the final electron density projection, the third being swamped out by the nearness of the oxygen atom. Figure 3 represents the difference map which shows three peaks surrounding the nitrogen atom. These peaks are at distances less than 1 Å from the nitrogen atom. Making use of the assumption that the N-H distance is 1 Å and the fact that the hydrogens surround the nitrogen tetrahedrally, positions were assigned to the hydrogen atoms. When the structure factors were calculated with the contributions of the hydrogen taken into consideration the agreement between the calculated and observed structure amplitudes of low angle reflexions improved considerably and, in fact, the discrepancy factor was $0{\cdot}136$. Perhaps it is worth mentioning that the co-ordinates assigned to the hydrogen atoms are far less accurate than those of the other atoms. The present data, however, do not warrant an attempt at refining the hydrogen position. Due to overlap the y co-ordinate of the hydrogen atom in the general position could not be

found in the (*hko*) projection. But an approximate value for *y* was obtained assuming the N-H distance to be 1 Å and it was found that the H-N-H angle came to be very nearly the tetrahedral angle. The final (*xyz*) parameters (in fractional co-ordinates) of the atoms in the crystal are tabulated in Table II.

TABLE II

Atom	*x*	*y*	*z*
Cl	0·433	0·250	0·192
N	0·183	−0·250	0·167
O_1	0·321	0·250	0·054
O_2	0·575	0·250	0·096
O_3	0·421	0·044	0·300
O_4	0·421	0·456	0·300
H_1	0·242	−0·250	0·075
H_2	0·225	−0·250	0·275
H_3	0·117	0·896	0·183
H_4	0·117	0·604	0·183

The final electron density projection along the *b*-axis is shown in Fig. 1 together with its key diagram in Fig. 2.

8. ACCURACY

To get an idea of the accuracy of the atomic co-ordinates the value of R_2 in the expression[8]

$$R_2 = \frac{\sum_{hol} (|F_o| - |F_c|)^2}{\sum_{hol} |F_o|^2} \qquad (2)$$

was calculated. The R.M.S. error was found to be 0·0028 Å which, in the opinion of the author, appears to be too low an estimate of the actual errors that exist in the present work. This is probably because the equation (2) is strictly applicable to the case where there is no overlap and reflexions are numerous. It was found that the oxygen movements of the order of 0·01

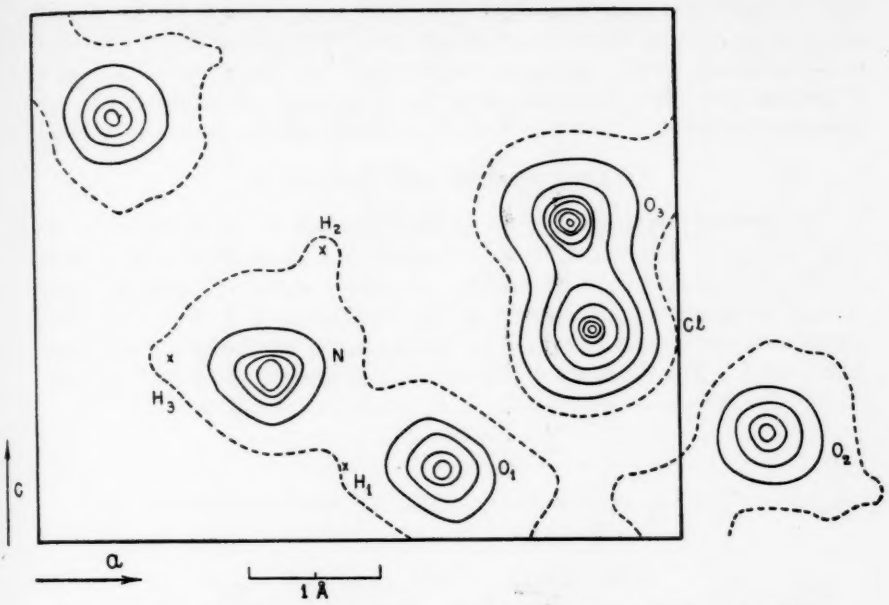

FIG. 1. The final electron density projection of NH_4ClO_4 on (010). Contour scale arbitrary.

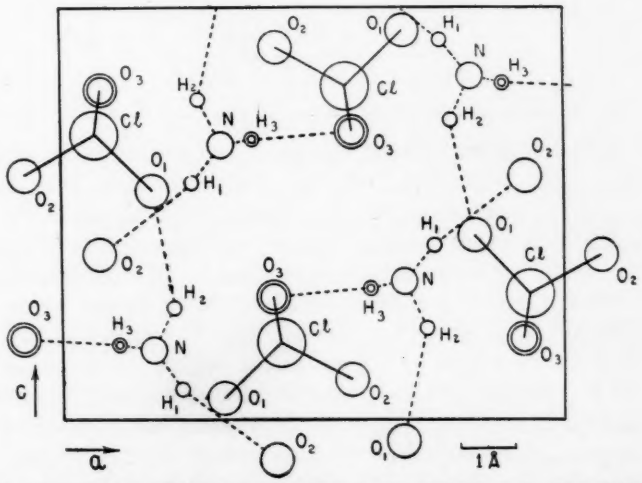

FIG. 2. A projection of the structure along *b*-axis of the crystal. Dotted lines represent hydrogen bonds.

to 0·02 Å from the present position had practically no effect on the discrepancy factor. It is, therefore, estimated that the errors in the co-ordinates of the different atoms would not exceed 0·02 Å. The observed structure amplitudes and those calculated using the final atomic co-ordinates are not given here for want of space but could be made available to anyone interested.

9. Discussion of the Structure

The general arrangement of the atoms in the unit cell is shown in Fig. 4. Each chlorine is surrounded by four oxygens at a mean distance of 1·46 Å and the four oxygens lie at the corners of a nearly regular tetrahedron. The average oxygen-to-oxygen distance in the tetrahedron is 2·37 Å. The distances between oxygens belonging to different ClO_4 tetrahedra are all larger than 3·24 Å. The distances inside the ClO_4 group are given in Table III.

Table III

	Cl–O	O–O
Distance in Å	1·45	2·34
	1·48	2·39
	1·45	2·37
	1·45	2·38
Mean ..	1·46 Å	2·37 Å

Each ammonium ion is surrounded by twelve oxygen atoms, the observed distances being 2·89, 2·93 (2×), 2·95 (2×), 2·95, 3·26 (2×), 3·39 (2×) and 3·15 Å (2×). It may be observed that six of these twelve oxygens are at a distance of about 2·95 Å which strongly suggest the presence of weak hydrogen bonds N-H ·· O. Such bonds have been reported in a few cases in the literature.[9, 10, 11] On the face of it there is a slight difficulty to say which of the four oxygen atoms out of the six are linked to the nitrogen by the N-H ·· O bonds, as there are two pairs of oxygen atoms which are at distances of 2·93 and 2·95 Å. But this difficulty is resolved if one assumes (i) that hydrogens satisfy the space group requirements, (ii) that they surround the nitrogen to form an approximate tetrahedron and (iii) that all the four oxygen atoms form hydrogen bonds. The four oxygens which could then be chosen uniquely as forming N-H ·· O bridges are those at distances of 2·89, 2·95

and 2·95 Å (2×). Such a choice is in accord with the disposition of the electron density maxima in the difference map.

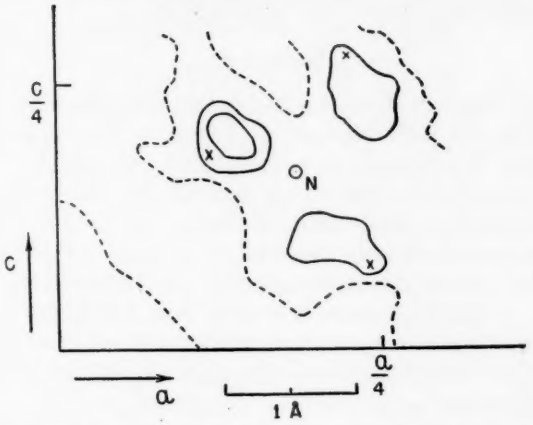

FIG. 3. (010) Difference map indicating approximate hydrogen positions. Contour scale arbitrary.

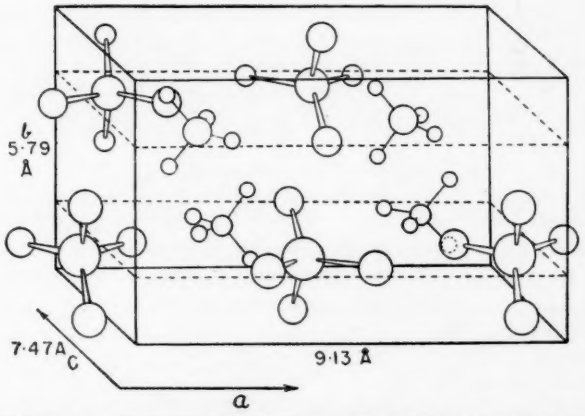

FIG. 4. The atomic arrangement in the crystal. The unit cell is outlined, and the stereoscopic effect is gained by assigning to an atom a diameter depending upon its Z co-ordinate.

In conclusion, it may be mentioned that the positions of the chlorine, oxygen and nitrogen atoms as determined by Gottfried and Schusterius (*loc. cit.*) are not far from those reported here. However, in the case of $KMnO_4$, contrary to the previous determination, the atomic co-ordinates are very close to those of NH_4ClO_4.

The author's grateful thanks are due to Professor R. S. Krishnan for his kind encouragement and continued interest, and to Dr. S. Ramaseshan for guidance and help throughout this investigation.

SUMMARY

The crystal structure of ammonium perchlorate has been redetermined. The orthorhombic cell with space-group *Pnma* has four molecules in a unit cell of dimensions $a = 9{\cdot}13$ Å, $b = 5{\cdot}79$ Å and $c = 7{\cdot}47$ Å. The values of the atomic co-ordinates have been refined by double Fourier-series methods and the final atomic positions determined are accurate to 0·02 Å. The positions of the hydrogen atoms have been obtained by the use of difference projection along the *b*-axis. In the structure each chlorine is surrounded tetrahedrally by four oxygen atoms at a mean distance of 1·46 Å. Each ammonium ion is surrounded by twelve oxygen atoms at distances varying from 2·89 to 3·39 Å. The four hydrogens surrounding each nitrogen form weak N-H··O bridges with the nearest oxygen atoms. Tables are given for various atomic co-ordinates and interatomic distances.

REFERENCES

1. Gottfried, C. and Schusterius, C. — *Zeit. Krist.*, 1933, **84**, 65.
2. Mooney, R. C. L. .. *Phys. Rev.*, 1931, **37**, 1306.
3. Wyckoff, R. W. G. .. *The Structure of Crystals*, 1935, Reinhold.
4. Ramaseshan, S., Venkatesan, K. and Mani, N. V. — *Proc. Ind. Acad. Sci.*, 1957, **46 A**, 95.
5. Barker, Th. V. .. *Zeit. Krist.*, 1907, **43**, 533.
6. Henry, N. F. M. and Lonsdale, K. — *International Tables for X-Ray Crystallography*, 1952, **1**, 408.
7. Hughes, E. W. .. *J. Am. Chem. Soc.*, 1941, **63**, 1737.
8. Booth, A. D. .. *Phil. Mag.*, 1945, **36**, 609.
9. Romers, C., Ketelaar, J. A. A. and MacGillavry, C. H. — *Acta Cryst.*, 1951, **4**, 114.
10. Van Niekerk, J. N. and Schoening, F. R. L. — *Ibid.*, 1952, **5**, 475.
11. Duke, J. R. C. and Llewellyn, F. J. — *Ibid.*, 1950, **3**, 305.

THE CRYSTAL STRUCTURE OF POTASSIUM PERCHLORATE—$KClO_4$

By N. V. Mani

(*Department of Physics, Indian Institute of Science, Bangalore* 3)

Received May 10, 1957

(Communicated by Dr. R. S. Krishnan, F.A.SC.)

1. Introduction

Although the crystal structures of $KClO_4$[1] and its isomorphs NH_4ClO_4[1] and $KMnO_4$[2] have been reported much earlier, very grave doubts as to the accuracy of the published parameters have been expressed in the litereture (Wyckoff[3]). Recent studies in this laboratory on the detailed analysis of the structures of $KMnO_4$[4] and NH_4ClO_4[5] have established that the previous determinations were far from correct. In view of this, a re-investigation of the structure of $KClO_4$ was carried out. The results of the analysis are presented in this paper.

From morphological studies this crystal is known to belong to the Orthorhombic bipyramidal class with axial ratios $a:b:c = 0{\cdot}7817:1:1{\cdot}2792$ (Groth[6]). The crystal is found to belong to the space-group *Pnma* with cell edges $a = 8{\cdot}83$ Å, $b = 5{\cdot}65$ Å, $c = 7{\cdot}24$ Å with four molecules in its unit cell. These data given by the previous workers are well in accord with those derived from the present measurements.

2. Determination of the Structure

Crystals of nearly circular cross-section were used with CuKα radiation, the intensity data about *b*- and *c*- axis were collected on zero-layer Weissenberg photographs using the multiple film technique. The intensities were estimated with care by visual comparison with standard scale and were corrected for Lorentz and polarisation factors and also for absorption using the Bradley's Tables for cylindrical specimen.

(*a*) (*hol*) *Projection*.—The knowledge of the parameters of the isomorph $KMnO_4$ determined in this laboratory was used to initiate the structure analysis of this crystal. The *b*-axis projection was taken up first because the (*hol*) zone contained the maximum number of reflexions. The structure factors were evaluated using atomic co-ordinates of the corresponding atoms in $KMnO_4$. The temperature and scale factors were estimated by plotting the logarithm of the ratio $\Sigma|F_o|/\Sigma|F_c|$ against $\sin^2\theta$, the summations being taken over increments of 0·2 in $\sin^2\theta$ (Wilson[7]). An isotropic temperature

factor exp. $[-B(\sin\theta/\lambda)^2]$ with the coefficient $B = 3{\cdot}8$ Å^2 and a scale factor of value 0·7 derived from the graph were employed for the first calculation of structure factors. When the discrepancies in the agreement of the observed and the calculated values are expressed as $\Sigma\{|F_c| - |F_o|\} \div \Sigma|F_o|$, the resultant value for this index at this stage amounted to 0·26 (a few reflexions which were found to be too weak to be observable were not taken into account in the calculation of the R-index).

From the first computations of the structure amplitudes the signs of 35 fairly strong reflexions out of a total of about 80 could be fixed with certainty. These reflexions were employed to construct the first difference Fourier synthesis parallel to (010) plane using the relevant electron density expressions for the space group *Pnma*. The computations were made at intervals of 6° with the aid of Beevers-Lipson strips. The resulting map indicated definite movements of the chlorine and oxygen atoms O_1 and O_2. On making these movements, the discrepancy index was found to become less. After performing three successive difference syntheses and effecting the movements of the atoms on the basis of these maps, the final structure factors were calculated. An estimate of the R-index at every stage provided the necessary check on the progress of the refinement.

An examination of the final structure factors showed that the calculated value of some of the strong reflexions were very much higher than the observed ones. This was believed to be due to extinction effects. The usual correction was made for this. The extinction coefficient was derived from a plot of $I_{calc.}/I_{obs.}$ *versus* $I_{calc.}$ for these reflexions which suffer extinction. After applying the correction, an estimate of the discrepancy index R for all reflexions recorded in this zone amounted to 0·154.

(*b*) (*hko*) *Projection.*—Space group considerations fixed the *y* parameters of the potassium, chlorine and the two oxygens of the ClO_4 group which placed them on reflexion planes at $\frac{3}{4}$ and $\frac{1}{4}$ along *b*-axis. The other two oxygen atoms of the perchlorate group are off the reflexion planes, one being the mirror-image of the other. The *y* co-ordinates of these two atoms remained to be fixed. The *c*-axis data were used in this determination.

Here again the corresponding value for this parameter derived in the case of $KMnO_4$ was utilised. The initial agreement between the structure factors was fairly good, as evident from the low value of the R (0·145). An attempt to refine the *y* parameter by the least squares method (Hughes[8]) yielded no effective change.

3. Diffraction Effects

At this stage of the work a Fourier synthesis projection on the *ac* plane was made using all the reflexions recorded. The contour map reproduced in Fig. 1 clearly indicates that the electron density maxima corresponding to the heavy atoms K and Cl and the oxygens O_3 (O_3 represents the two atoms O_3 and O_4 which overlap in this projection) appeared at the position arrived at by the difference synthesis technique. On the other hand, the positions of

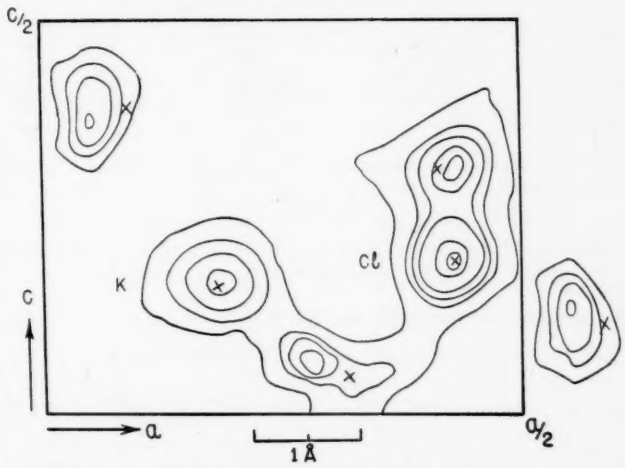

Fig. 1. *b*-axis Fourier projection of $KClO_4$ using all the reflections recorded with CuKα demonstrating the prominent diffraction effects: Contours drawn at arbitrary intervals.

the peaks due to the other two oxygens O_1 and O_2 were considerably displaced from the positions assigned to them in the unit cell. A small shift in the co-ordinates of these oxygen atoms in the direction of the maxima spoiled the good agreement obtained previously between the observed and calculated amplitudes. This very strongly suggested that the displacement of the electron density maxima in the Fourier projection was, to a large extent, caused by diffraction effects rather than due to any inaccuracy in the atomic positions.

To confirm that this discrepancy arises as a result of diffraction errors, the contributions due to K and Cl atoms were removed from the structure factors (with the relevant temperature factor applied) and the resultant coefficient was used to construct a Fourier map. The peaks in this diagram (Fig. 2) which correspond to oxygen atoms O_1 and O_2 very nearly coincided with their respective positions derived previously and the electron density contours approximated closely to circles.

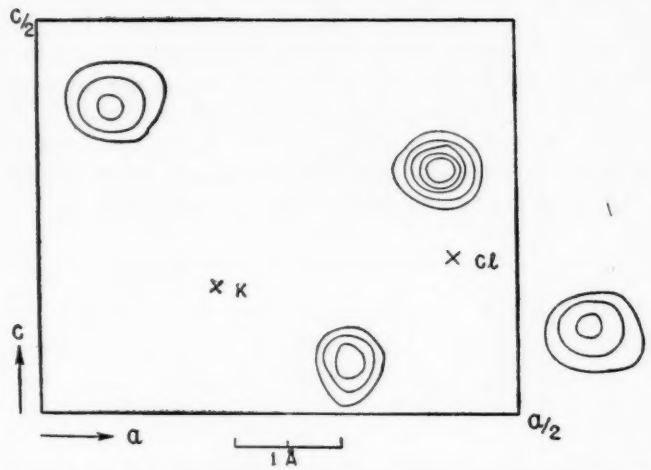

FIG. 2. Elimination of diffraction errors: *b*-axis Fourier projection with contributions due to K and Cl atoms removed. Contours drawn at arbitrary intervals.

It is reasonable to expect this since it is quite obvious that the error arising as a result of the ' termination of series ' is automatically corrected for when difference synthesis technique is employed in the analysis of a structure. But it is thought worthwhile in this connection to focus attention on the diffraction effects particularly as these are found to be inordinately large in the present case.

Finally, a difference synthesis with the heavy atom contributions (K and Cl) removed from the structure factor was performed in an endeavour to refine the oxygen parameters further still. Various movements based on this computed map as well as on trial were made, and none of these movements, either individually or in co-ordination, did help to improve the structure. A different temperature factor on oxygens 1 and 2, as suggested by the map, was also tried and this improved the value of the R-index to a small extent. The fact that the effective value of the index ($R = 0{\cdot}234$) was appreciably higher than the corresponding value ($R = 0{\cdot}154$) calculated for the complete structure needs particular mention here.

Further attempts to refine the parameters were not carried out as it was felt that the uncertainty regarding the experimental intensities did not warrant it. Table I gives the observed structure factors and those calculated with the final atomic positions.

4. The Discussion of the Structure

The atomic parameters expressed in fractional co-ordinates are given with reference to a centre of symmetry as the origin and the other co-ordi-

Table I

Comparison of observed and calculated structure factors

hkl	F_o	F_c	*hkl*	F_o	F_c
000	..	272	405	30·1	−28·5
002	63·5	−68·6	406	5·4	− 3·3
004	17·4	−22·0	407	21·2	18·4
006	30·0	29·1	408	2·9	1·9
008	24·8	−16·4	501	8·8	11·9
200	16·1	16·0	502	11·2	13·6
400	32·4	−33·6	503	24·2	−24·9
600	17·2	−16·2	504	4·4	6·8
800	49·0	−40·0	505	0	1·6
10,00	0	3·5	506	5·5	− 5·9
101	15·3	−16·8	507	6·7	6·7
102	41·0	−44·2	508	4·8	4·1
103	8·5	13·9	601	0	0
104	14·2	14·3	602	17·1	19·8
105	5·5	− 2·3	603	5·1	5·1
106	5·0	− 3·5	604	4·9	− 5·2
107	6·6	6·9	605	0	7·1
108	9·0	−10·1	606	0	1·1
109	0	1·8	607	0	1·4
201	28·4	29·9	701	0	4·2
202	24·8	−29·8	702	25·5	−23·7
203	26·4	−33·2	703	7·8	− 9·4
204	9·2	9·7	704	12·3	−11·2
205	14·9	17·1	705	0	1·2
206	0	− 2·5	706	0	− 1·9
207	8·6	11·9	707	4·8	2·3
208	5·4	− 5·8	801	10·7	− 9·4
209	9·0	− 8·3	802	15·7	14·5
301	9·7	−11·7	803	4·5	7·0
302	26·0	−29·8	804	5·8	5·8
303	46·4	48·6	805	5·1	3·7
304	7·3	3·3	806	12·6	−10·0
305	12·2	− 9·9	901	0	1·9
306	6·5	− 7·6	902	8·5	5·5
307	7·6	− 7·7	903	0	0
308	0	2·0	904	5·9	−4·2
309	4·7	3·8	905	3·2	4·0
401	88·2	76·4	10,01	0	−2·8
402	9·6	9·4	10,02	0	−0·4
403	33·4	−32·2	10,03	0	5·4
404	0	4·2	10,04	0	−2·7

TABLE I—(*Contd.*)

hkl	F_o	F_c	*hkl*	F_o	F_c
020	81·3	−94·4	610	23·5	28·2
040	60·0	65·9	620	7·8	−12·2
060	21·2	−19·8	630	16·0	−18·5
200	22·9	15·9	640	3·8	− 3·4
400	39·2	−32·4	650	cut off	8·5
600	13·5	−15·0	660	0	− 0·6
800	35·1	−34·5	810	0	2·7
10,00	0	3·0	820	24·6	21·9
210	74·4	82·7	830	4·7	− 6·3
220	21·2	21·9	840	20·2	−15·7
230	29·6	−27·2	850	0	0
240	0	1·9	10,10	13·6	−11·7
250	27·5	23·5	10,20	0	0
260	0	1·1	10,30	9·3	6·6
270	6·7	− 4·3			
410	23·1	−25·4			
420	3·2	3·0			
430	27·8	26·1			
440	7·6	− 9·0			
450	3·0	− 1·2			
460	2·9	2·0			

nates follow from a consideration of symmetry of space group *Pnma*. The corresponding values obtained by the earlier workers are also listed in Table II for sake of comparison.

TABLE II

Atom	Present work			Previous work		
	x	*y*	*z*	*x*	*y*	*z*
K	0·183	0·75	0·158	0·192	0·75	0·167
Cl	0·433	0·25	0·192	0·425	0·25	0·189
O_1	0·321	0·25	0·046	0·325	0·25	0·050
O_2	0·583	0·25	0·108	0·578	0·25	0·106
O_3	0·417	0·037	0·308	0·417	0·042	0·319
O_4	0·417	0·463	0·308	0·417	0·458	0·319

It can be noticed that the atomic co-ordinates derived from the present investigation are appreciably different from those reported by the previous workers—particularly the values of the x co-ordinates of Cl and K and the z co-ordinates of K and O_8 (oxygens which are in general positions) show significant changes which are found to be beyond the limits of probable errors. Hence these variations can be taken to be genuine.

Each chlorine atom is surrounded by four oxygen atoms at a mean distance of 1·46 Å and these atoms lie at the corners of an almost regular tetrahedron. The average O—O distance is 2·39 Å and the shortest distance is 2·36 Å . The distances between oxygen atoms belonging to different ClO_4 tetrahedra are all greater than 3·25 Å. The Cl—O and the O—O distances in one ClO_4 group are given in Table III. The corresponding values of the previous workers are also listed.

TABLE III

	Present work	Previous work
$Cl—O_1$	1·45 Å	1·34 Å
$Cl—O_2$	1·46	1·48
$Cl—O_3$	1·48	1·51
$O_1—O_2$	2·36	2·27
$O_2—O_8$	2·39	2·41
$O_8—O_1$	2·41	2·42
$O_3—O_4$	2·40	2·35

It is interesting to compare the various inter-atomic distances obtained in the case of NH_4ClO_4[5] with the present crystal. In NH_4ClO_4 the mean Cl—O and O—O distances are 1·46 Å and 2·37 Å respectively. These values compare favourably with those reported above. In addition it may be mentioned that Cl—O distance in $NaClO_4$ is 1·51 Å and the mean O—O distance is 2·51 Å (Zachariasen[9]).

Each potassium ion is surrounded by twelve oxygen atoms at an average distance of 3·1 Å and the shortest distance between an oxygen atom and a K ion is 2·88 Å.

It is of considerable interest from the point of view of the structure as well as the properties of this substance to know the exact shape of the ClO_4 and MnO_4 groups to ascertain whether the tetrahedra are perfect or not. This knowledge would be invaluable to explain the pleochroism exhibited by $KMnO_4$.[4] But with the the data available, it is not possible to state anything definite about this—for example, in the case of $KMnO_4$ when Mn—O distances were altered from 1·6 Å to 1·56 Å, the R-value changed from 0·156 to 0·150 only. Similar results have been obtained in the case of ClO_4 tetrahedron in $KClO_4$ and in NH_4ClO_4. It is only possible to assert that the Cl—O or Mn—O distance is not different from those given in Table III by more than 4 or 5 %.

Finally it may be mentioned that the structure of $KClO_4$ closely resembles that of its isomorphs $KMnO_4$ and NH_4ClO_4.

The author wishes to express his gratitude to Professor R. S. Krishnan for his kind encouragement and to Dr. S. Ramaseshan for guidance and help throughout this investigation.

SUMMARY

The crystal structure of $KClO_4$ has been completely redetermined. The atomic parameters are found to be different from those reported previously for this crystal. The crystals are orthorhombic with space group *Pnma* and 4 molecules in a cell of edges $a = 8·83$ Å, $b = 5·65$ Å and $c = 7·24$ Å. The analyses of the structure and the refinement of parameters were carried out by the iteration process of difference synthesis technique. The very prominent diffraction effects encountered in the present case has been pointed out. A procedure involving removal of heavy atom contributions from the structure factors and the computation of Fourier map utilising these coefficients, was adopted to confirm the existence of these diffraction effects. The final discrepancy index calculated for the (*hol*) and (*hko*) zones were found to be 0·156 and 0·145 respectively. This value estimated after the removal of the heavy atoms K and Cl from the structure, amounted to 0·235. In the structure each chlorine atom is surrounded by 4 oxygens at a mean distance of 1·46 Å which lie at the corners of a nearly regular tetrahedron with Cl at the centre. Each K ion is surrounded by 12 oxygen atoms at an average distance of 3·1 Å . Tables are given for the various atomic co-ordinates and inter-atomic distances. Similarity of this structure to its two isomorphs has been pointed out.

References

1. Gottfried, C. and Schusterius, C. — *Zeit. Kristallogr.*, 1933, **84**, 65.
2. Mooney, R. C. L. .. *Phys. Rev.*, 1931, **37**, 1306.
3. Wyckoff, R. W. G. .. *Structure of Crystals*, (Reinhold), 1935, 72.
4. Ramaseshan, S., Venkatesan, K. and Mani, N. V. — *Proc. Ind. Acad. Sci.*, 1957, **46**, 95.
5. Venkatesan, K. .. *Ibid.*, 1957, **46**, 134.
6. Groth, P. .. *Chemische Krystallographe*, **2**, 167 (Leipzig, Engelmann).
7. Wilson, A. J. C. .. *Nature* (London), 1942, **150**, 152.
8. Hughes, E. W. .. *Jour. Amer. Chem. Soc.*, 1941, **63**, 1737.
9. Zachariasen, W. H. .. *Zeit. Kristallogr.*, 1930, **73**, 141.

THE VAN DER WAAL'S INTERACTION OF ANISOMETRIC COLLOIDAL PARTICLES

By Marjorie J. Vold*

(*Department of General Chemistry, Indian Institute of Science, Bangalore-3*)

Received June 6, 1957

(Communicated by Dr. S. Bhagavantam, F.A.SC.)

1. Introduction

The currently accepted theory of the stability of aqueous lyophobic colloidal sols[6] is based squarely on the hypothesis that the particles are subject to an attraction derivable by summing up the van der Waal's interaction between all pairs of atoms in the two particles. Irreversible coagulation occurs when the electrical repulsion is reduced by addition of electrolyte so that this attraction becomes dominant. Precise evaluation of the dependence of the repulsion on electrolyte concentration is more important to quantitative applications of the theory than is precise evaluation of the van der Waal's terms.

However an important group of colloids exists for which more elaborate analysis of the van der Waal's effects is useful. Examples are furnished by suspensions of metal soaps in hydrocarbons (lubricating greases)[8] and ore slimes.[4] The primary colloidal particles are believed to be solvated but not permeated or swollen by solvent as is the case for many true lyophilic colloids. The occurrence of a solvent sheath preventing very close approach of particles is possibly responsible for the partial failure of the conclusions of Koelmans and Overbeek[3] regarding the relative roles of electrical and steric effects in stabilizing colloidal suspensions, in relation to the size of the particle. Mechanically reversible flocculation occurs in this type of suspension and is explicable on the supposition that at the limiting separation dictated by the solvation, the van der Waal's interaction is of the same order of magnitude as local shear stresses. Many other properties can be described plausibly if only suitable assumptions are made concerning the magnitude of the van der Waal's interaction and its probable dependence on the inter-particle distance. Hence a calculation is needed to justify such speculations.

Since to a first approximation the attraction varies with the inverse sixth power of the separation of atoms, it is apparent that the sum over all atom pairs in two particles will depend critically on the shape and mutual orientation of the particles. Following the original discussion for spherical particles

* Permanent Address: Department of Chemistry, University of Southern California, Los Angeles, California, U.S.A.

by Hamaker[2] a number of attempts have been made to evaluate the interaction for other shapes[1,7] but the restrictions on shape (as infinitely thin discs, infinitely long rods of rectangular cross-section) and limited range of orientations (as mutually parallel or perpendicular) introduced in the attempt to obtain an exact result for the required integrals has severely limited their utility.

In the present work the interaction between ellipsoidal particles of arbitrary size and axial ratios in any mutual orientation has been evaluated by the strategem of expanding the interaction in inverse powers of the separation of the centres of mass of the particles. Although the resultant series converges only slowly at small separations, the results have already proven useful in analyzing the properties of suspensions of metal soaps in hydrocarbons.

2. Derivation of the Interaction Energy

The two particles are taken as ellipsoids with semi-axes a, b, c and α, β, γ respectively. The expression to be evaluated is

$$V = - \wedge \iint \frac{dv_1 dv_2}{r^6} \tag{1}$$

where the constant $\wedge$ is taken as $n_1 n_2 \lambda_{12}$, n_1 and n_2 being the numbers of atoms with interaction constant λ_{12} per cubic centimeter in each of the two particles of volume elements dv_1 and dv_2, and r is the distance between the volume elements. Note that this $\wedge$ is less than the "A" of the extensive series of papers of Overbeek and colleagues by the factor π^2, although the significance of λ_{12} is unchanged.

Reference to Fig. 1 shows that the separation r can be described in terms of the separation of the centres of mass of the particles, R, and the direction cosines of R and of the axes of which points in the second ellipsoid are referred, relative to the axes to which points in the first ellipsoid are referred.

$$r^2 = (x'' - x)^2 + (y'' - y)^2 + (z'' - z)^2 \tag{2}$$

$$\left.\begin{aligned} x'' &= l_1 x' + m_1 y' + n_1 z' + \mathrm{R}\cos\theta\sin\phi \\ y'' &= l_2 x' + m_2 y' + n_2 z' + \mathrm{R}\sin\theta\sin\phi \\ z'' &= l_3 x' + m_3 y' + n_3 z' + \mathrm{R}\cos\phi \end{aligned}\right\} \tag{3}$$

By substituting (3) in (2) and rearranging terms, r^{-6} can be written as:

$$r^{-6} = \mathrm{R}^{-6}(1 + \mathrm{S} + \mathrm{T})^{-3} \tag{2 a}$$

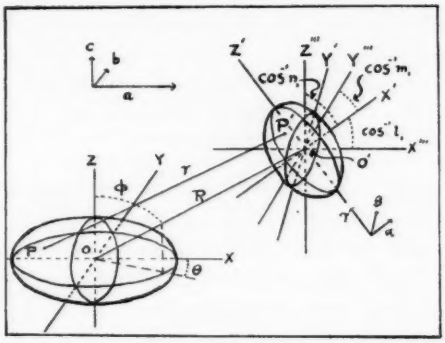

FIG. 1. Co-ordinate System and Nomenclature for Calculation of the Interaction of Two Ellipsoids.

0 is the origin. r, the separation of two arbitrary points is first expressed as the distance PP′ referred to 0, and then the co-ordinates of P′ are expressed in terms of x', y' and z' referred to 0′ and the translation along R and rotations about x''', y''' and z''' needed to superpose the two sets of axes. (Only one of the three sets of direction cosines, l, m, n, is shown.) α, β, γ and a, b, c are the semi-axes of the two ellipsoids.

where S is of order x/R and T is of order x^2/R^2, x being used here to refer to any of the six co-ordinates. This expression is then expanded to yield

$$r^{-6} = \mathrm{R}^{-6} \sum_{k=0}^{\infty} \sum_{l=0}^{k} \frac{(-1)^k (2+k)!\, \mathrm{S}^{k-l}\mathrm{T}^l}{2l!\,(k-l)!} \qquad (2\,b)$$

Each term of this double sum will itself be a multiple sum with terms of the form

$$\mathrm{R}^{-(k+l)}\, \mathrm{C}(k, l, m_i)\, x^{m_1} y^{m_2} z^{m_3} x'^{m_4} y'^{m_5} z'^{m_6}$$

where

$$\sum_{i=1}^{6} m_i = k + l$$

These can be readily integrated over the volumes of the ellipsoids,

$$\frac{x^2}{a^2} + \frac{y^2}{b^2} + \frac{z^2}{c^2} = 1$$

and

$$\frac{x'^2}{\alpha^2} + \frac{y'^2}{\beta^2} + \frac{z'^2}{\gamma^2} = 1 \qquad (4)$$

the general expression being

$$\int\int\int x^{2u}y^{2v}z^{2w}dx\,dy\,dz$$

$$= \frac{a^{2u+1}b^{2v+1}c^{2w+1}\Gamma(u+\frac{1}{2})\,\Gamma(v+\frac{1}{2})\,\Gamma(w+\frac{1}{2})}{\Gamma(u+v+w+5/2)} \tag{5}$$

In continuing the expansion of (2 *b*) in order to obtain the various coefficients $C(k, l, m_i)$ it is convenient to discard terms in which any co-ordinate occurs to an odd power as soon as it appears since these will all vanish in the integration process any way. It is also convenient to introduce a somewhat compact nomenclature as follows:

$$\left.\begin{aligned}
&A = \sum_{r=1}^{3}\sigma_r x_r \qquad B = \sum_{s=1}^{3} x_s^2 \qquad C = \sum_{t=1}^{3} q_t x_t\\
&A' = \sum_{r'=1}^{3}\sigma'_{r'}x'_{r'} \qquad B' = \sum_{s'=1}^{3} x'^2_{s'} \qquad C' = \sum_{t'=1}^{3} q'_{t'}x'_{t'}
\end{aligned}\right\}$$

where x_1, x_2, x_3 replaces x, y, z and x_1', x_2', x_3' replaces x', y', z' and

$$\left.\begin{aligned}
&\sigma_1 = \cos\theta\sin\phi \qquad \sigma_2 = \sin\theta\sin\phi \qquad \sigma_3 = \cos\phi\\
&\sigma_1' = l_1\cos\theta\sin\phi + l_2\sin\theta\sin\phi + l_3\cos\phi\\
&\sigma_2' = m_1\cos\theta\sin\phi + m_2\sin\theta\sin\phi + m_3\cos\phi\\
&\sigma_3' = n_1\cos\theta\sin\phi + n_2\sin\theta\sin\phi + n_3\cos\phi\\
&q_1q_1' = l_1 \qquad q_1q_2' = m_1 \qquad q_1q_3' = n_1\\
&q_2q_1' = l_2 \qquad q_2q_2' = m_2 \qquad q_2q_3' = n_2\\
&q_3q_1' = l_3 \qquad q_3q_2' = m_3 \qquad q_3q_3' = n_3
\end{aligned}\right\} \tag{6}$$

The change in notation, followed by substitution of (3) in (2), leads to the result

$$S = \frac{2(A'-A)}{R}\,; \quad T = \frac{B+B'}{R^2} - \frac{2CC'}{R^2}$$

$$r^{-6} \doteq R^{-6}\sum_{n=0}^{\infty}\sum_{l=0}^{n} \times \frac{R^{-2n}(-1)^l(2+2n-l)!\,2^{2n-2l-1}(A'-A)^{2n-2l}(B+B'-2CC')^l}{l!\,(2n-2l)!} \tag{7}$$

The symbol $\doteq$ in place of $=$ is written as a reminder that by setting the index $k = 2n - l$ some odd powers of co-ordinates have already been dropped out.

The next step is to introduce the explicit values of A, A′ etc., and collect the coefficients of similar terms. The result can be written

$$r^{-6} \doteq \mathrm{R}^{-6} \sum_{n=0}^{\infty} \sum_{p=0}^{n} (-1)^p \, \mathrm{R}^{-2n} 2^{2n-2p-1} (2n+2-p)! \times \sum_{i_m j_m k_m} 2^{\delta} \delta! \prod_{m=1}^{6} \frac{\sigma_m{}^{2j_m - k_m} q_m{}^{k_m} x_m{}^{2i_m}}{(2j_m - k_m)! \, k_m! \, (i_m - j_m)!} \tag{8}$$

In this expression x_1', x_2', x_3' and the corresponding σ's and q's have been replaced by x_4, x_5, x_6, etc. In carrying out the sum over the $3 \times 6 = 18$ indices $i_m j_m k_m$ the possible choices of indices are as follows:

$$\left.\begin{array}{lll} 0 \leqslant i_m \leqslant n & \sum_{m=1}^{6} i_m = n & \\ 0 \leqslant j_m \leqslant i_m & \sum_{m=1}^{6} j_m = n - p + \delta & \\ 0 \leqslant k_m \leqslant 2j_m & \sum_{m=1}^{6} k_m = 2\delta & \delta = k_1 + k_2 + k_3 \end{array}\right\} \tag{9}$$

For $n = 0$ there is only one surviving term, which is unity. For $n = 1$ any of the six i values can be unity with the remainder zero. The j_m corresponding to $i_m = 1$ can be zero or unity, but all k_m can only be zero. Further, for $p = 0$ the j_m corresponding to $i_m = 1$ must be unity and cannot be zero while for $p = 1$ all j_m are zero. Hence there will be six terms of the form

$$(24\sigma_m{}^2 - 3) \, x_m{}^2 \, \mathrm{R}^{-2}$$

Application of equations (1) and (5) to these first two values of n leads to the series

$$\mathrm{V} = - \wedge \cdot \frac{16\pi^2 abc \, \alpha\beta\gamma}{9} \left\{ 1 + \sum_{m=1}^{6} \frac{24\sigma_m{}^2 - 3}{5\mathrm{R}^2} \, a_m{}^2 + \ldots . \right\}$$

(where a_m represents each of the six semi-axes).

Proceeding in a similar fashion the final result is obtained

$$\mathrm{V} = - \frac{\wedge v_1 v_2}{\mathrm{R}^6} \sum_{n=0}^{\infty} v_n \mathrm{R}^{-2n} \tag{10}$$

where v_1 and v_2 are the volumes of the two ellipsoids and

$$\begin{aligned} v_0 &= 1 \\ v_1 &= \Sigma \, c_i a_i{}^2 \\ v_2 &= \Sigma \Sigma \, c_{ij} a_i{}^2 a_j{}^2 \\ &\vdots \\ v_n &= \Sigma \Sigma \cdots \Sigma \, c_{ij \ldots s} \, a_i{}^2 a_j{}^2 \ldots a_s{}^2 \end{aligned}$$

The indices $i, j, \ldots . s$ run from 1–6 with

$$c_i = \frac{24}{5}\sigma_i^2 - \frac{3}{5}$$

$$\begin{cases} c_{ii} = \frac{144}{7}\sigma_i^4 - \frac{72}{7}\sigma_i^2 + \frac{18}{35} & (a) \\ c_{ij} = \frac{144}{7}\sigma_i^2\sigma_j^2 - \frac{12}{7}(\sigma_i^2 + \sigma_j^2) + \frac{6}{35} & (b) \\ c_{ij} = \frac{144}{5}\sigma_i^2\sigma_j^2 - \frac{12}{5}(\sigma_i^2 + \sigma_j^2) + \frac{6}{25} \\ \qquad - \frac{48}{5}\sigma_i\sigma_j l_{ij} + 12 l^2{}_{ij} & (c) \end{cases}$$

Note that c_{ij} is given by three types of expression according as $i = j$ (*a*) or $i \neq j$ but a_i and a_j are semi-axes of the same ellipsoid (*b*) or $i \neq j$ and a_i and a_j are semi-axes of different ellipsoids (*c*).

Note also that the l, m, n of the original notation used in (3) is here replaced by the 36 membered set l_{ij} given by

$$l_{ij} = \begin{pmatrix} 0 & 0 & 0 & l_1 & l_2 & l_3 \\ 0 & 0 & 0 & m_1 & m_2 & m_3 \\ 0 & 0 & 0 & n_1 & n_2 & n_3 \\ l_1 & m_1 & n_1 & 0 & 0 & 0 \\ l_2 & m_2 & n_2 & 0 & 0 & 0 \\ l_3 & m_3 & n_3 & 0 & 0 & 0 \end{pmatrix}$$

The values for c_{ijk} fall into 5 categories depending on whether $i = j = k$ (*a*) or two indices are alike (*b* and *c*) or no two alike (*d* and *e*). For case (*b*) both a_i and a_k are semi-axes of the same ellipsoid while in case (*c*) they are semi-axes of different ellipsoids. Cases (*d*) and (*e*) differ correspondingly from each other.

$$c_{iii} = \frac{256}{3}\sigma_i^6 - 80\sigma_i^4 + \frac{120}{7}\sigma_i^2 - \frac{10}{21} \qquad (a)$$

$$c_{iik} = \frac{256}{3}\sigma_i^4\sigma_k^2 - \frac{16}{3}\sigma_i^4 - 32\sigma_i^2\sigma_k^2 + \frac{16}{7}\sigma_i^2 + \frac{8}{7}\sigma_k^2 - \frac{2}{21} \qquad (b)$$

$$c_{iik} = \frac{768}{5}\sigma_i^4\sigma_k^2 - \frac{48}{5}\sigma_i^4 - \frac{288}{5}\sigma_i^2\sigma_k^2 + \frac{144}{35}\sigma_i^2 + \frac{72}{35}\sigma_k^2 - \frac{6}{35} - \frac{384}{5}\sigma_i^3\sigma_k l_{ik} + \frac{576}{35}\sigma_i\sigma_k l_{ik} + \frac{288}{5}\sigma_i^2 l^2_{ik} - \frac{24}{35}l^2_{ik} \qquad (c)$$

$$c_{ijk} = \frac{256}{3}\sigma_i^2\sigma_j^2\sigma_k^2 - \frac{16}{3}(\sigma_i^2\sigma_j^2 + \sigma_i^2\sigma_k^2 + \sigma_j^2\sigma_k^2) + \frac{22}{63} \qquad (d)$$

$$c_{ijk} = \frac{768}{5}\sigma_i^2\sigma_j^2\sigma_k^2 - \frac{48}{5}(\sigma_i^2\sigma_j^2 + \sigma_i^2\sigma_k^2 + \sigma_j^2\sigma_k^2) + \frac{24}{35}(\sigma_i^2 + \sigma_j^2 + \sigma_k^2) - \frac{2}{35} - \frac{192}{5}(\sigma_i\sigma_j^2\sigma_k l_{ik} + \sigma_i^2\sigma_j\sigma_k l_{jk}) + \frac{96}{35}(\sigma_j\sigma_k l_{jk} + \sigma_i\sigma_k l_{ik}) + \frac{48}{35}(\sigma_j^2 l^2_{ik} + \sigma_i^2 l^2_{jk}) + \frac{192}{35}\sigma_i\sigma_j l_{ik} l_{jk} - \frac{4}{35}l^2_{ik} - \frac{4}{35}l^2_{jk} \qquad (e)$$

Note that each term c_{ij} appears as $C_{ij}\, a_i^2\, a_j^2$ and again as $C_{ji}\, a_j^2\, a_i^2$. Similarly each C_{iik} occurs three times and each C_{ijk} occurs six times.

In making numerical calculations it is convenient to observe that v_1 contains 6, v_2 21 and v_3 56 separate terms. The c's pertinent to particular orientations can then be tabulated, preferably on 6, 21 or 56 separate cards. The values of a_i^2, a_j^2, etc., for each shape of particle can be similarly arranged and the particular series for the interaction energy for a given shape and orientation obtained by leafing through the two sets of cards, multiplying and summing simultaneously on a desk calculator.

It is unfortunate that series such as (10) do not converge very rapidly for small particle separations and that the rate of convergence is dependent on particle shape and orientation. Hlowever, useful results can be obtained even with the first four terms here calculated, and the number of terms can be readily increased as needed. The series are not divergent for any values of orientation and separation such that the particles do not touch or intersect each other.

3. Numerical Results and Discussion

Sample calculations have been made for prolate spheroids (corresponding to rod- or needle-shaped particles), oblate spheroids (corresponding to disk- or plate-shaped particles) and for one effectively lath-shaped particle. The line joining the centres of gravity has been taken along the common X-axis ($\sigma_1 = \sigma_4 = 1$; $\sigma_2 = \sigma_3 = \sigma_5 = \sigma_6 = 0$) with the y and y' and z and z' axes mutually parallel.

Four typical curves are plotted in Fig. 2 for "rod-shaped" particles of equal size with a length to width ratio of 10 in (*a*) end-to-end orientation, (*b*) in an end-to-centre orientation, (*c*) with long axes parallel, and (*d*) with long axes mutually perpendicular and crossed as indicated in Fig. 2. Consideration of the original expression for V (eq. 1) leads directly to the qualitative expectation that for a fixed separation of the centres of mass, the end-to-end orientation (which results naturally in the smallest distance of closest approach of surfaces) will have the largest value of V, and that the two orientations in which the long axes lie in parallel planes will have the smallest value. The interest of Fig. 2 lies in the magnitude of the dispersion of values and the particle separation at which it becomes appreciable.

In making the numerical calculations which are represented on Figs. 2–8, the two particles have been taken with equal volumes and with the product of the semi-axes 0·01 arbitrary volume units for all shapes of particle. The separation of centres of mass R and distance of closest approach of surfaces (δ) are expressed in the corresponding arbitrary unit of length. Hence in evaluating the particle separation at which some effect occurs in this case, for example, the particle separation at which V begins to depend significantly upon mutual orientation, the ratio of R (or δ) to the cube root of particle volume (0·348) should be considered. Fig. 2 shows that for a length width ratio of 10, it is noticeable at ca. 15 times this value (R = 5 or R = 1500 Å for particles whose "mean diameter" is 0·1 micron). In this case the interaction energy varies by a factor of 10 between the most favourable and most unfavourable orientations when R has decreased to ca. $6 \times 0{\cdot}348$ (R = 2 or 600 Å).

In Fig. 3 the ratio of the maximum interaction energy (as a function of orientation) to the minimum interaction energy, for several values of the separation of centres of mass is plotted as a function of the length/width ratio of "rod-shaped" particles. It can be seen that the spread in values of V increases very sharply with increasing anisometry and that the spread reaches a given value at a lesser anisometry (axial ratio) when the particles are close together.

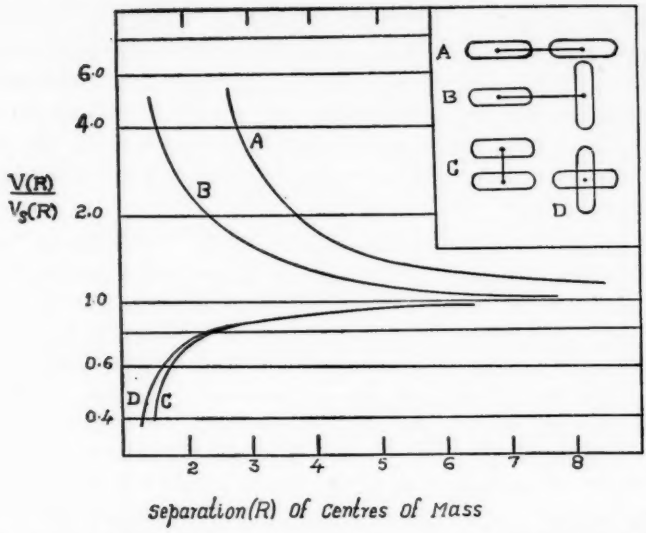

FIG. 2. Interaction energy of prolate spheroids with $a/b = 10$ relative to spheres of the same volume at the same separations of centres of mass in various orientations.
The insert, showing the particle orientations, applies also to Fig. 8.

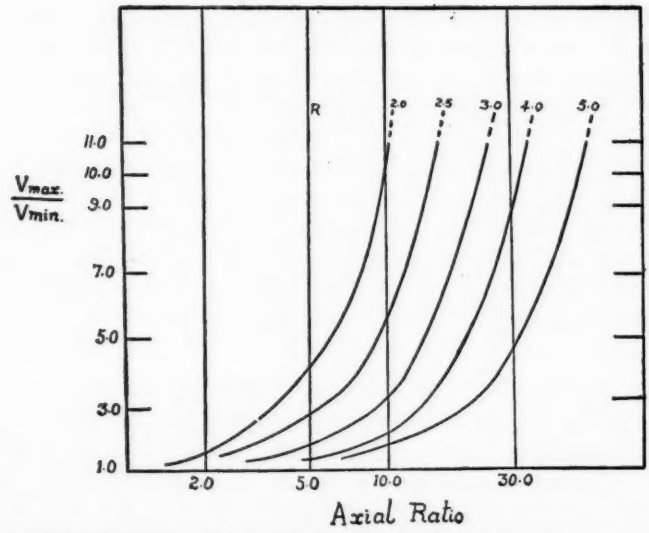

FIG. 3. Ratio of maximum interaction energy to minimum interaction energy (as a function of orientation) as it depends on the axial ratio of prolate spheroids at various separations of the centres of mass.

Figures 4 and 5 (for "disc-" and "lath-" shaped particles) show the same kind of effects. For oblate spheroids with $a/b = 10$ an orientation with the short axes parallel as indicated in Fig. 4 insert gives maximum interaction at a fixed separation of the centres of mass and an orientation with the long axes parallel gives minimum interaction. The spread between them increases with decreasing distance. It is slightly less pronounced at each separation than for prolate spheroids the same axial ratio, reaching a factor of 10 only at R/0·348 ca. 4·6 (R = 1·6). For simulated lath-shaped particles ($a:b:c = 100:10:1$), calculations were made for twelve orientations, which turned out to give three groups of curves. The spread between maximum and minimum interaction becomes large at much greater separations being already a factor of 10 at R/0·348 = 13 (R = 4·5).

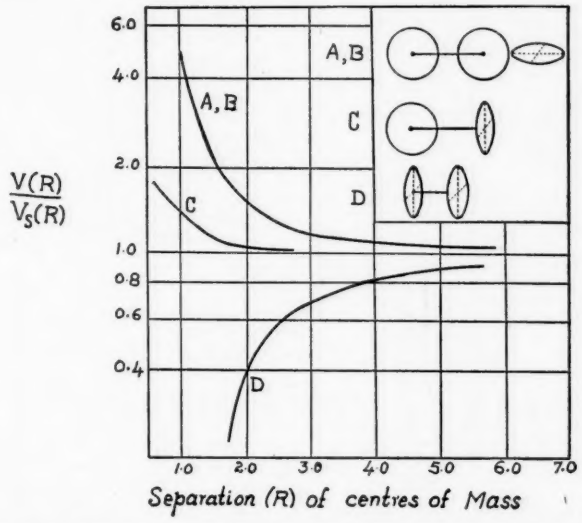

FIG. 4. Interaction energy of oblate spheroids with $a/b = 10$ in various orientations, relative to the interaction energy of spherical particles at the same separation of the centres of mass.

The insert, showing the orientations, applies also to Fig. 7.

In application to the behaviour of suspensions these interactions at constant separation of centres of mass are of importance in considering the effect of sol concentration, since the distribution of R values is determined in considerable part by this variable. If the particles in a sol are uniformly distributed the mean separation of centres of mass is of the order of $(V/n)^{\frac{1}{3}}$ where V is the volume containing n particles, or $(Cv_p)^{-\frac{1}{3}}$ where C is the volume

fraction of suspended material whose particle volume is v_p. Electron microscopic estimates for some sols of lithium stearate in *n*-heptane under study in this laboratory gave a mean volume of about 5×10^{-16} c.c. Hence in a one per cent. suspension $\bar{R}$ is of the order of 0·37 microns. $v_p^{\frac{1}{3}}$ is 0·08 μ so that the ratio is quite close to 4·5. These particles approximate closely to the shape chosen for Fig. 5. With a spread of a factor of 10 in the interaction energies, if the constant $\wedge$ is large enough, most of the particles will have "end-on" mutual orientations and, again if $\wedge$ is large enough, form a three-dimensional net-work which does not settle under gravity. This is exactly what is observed.

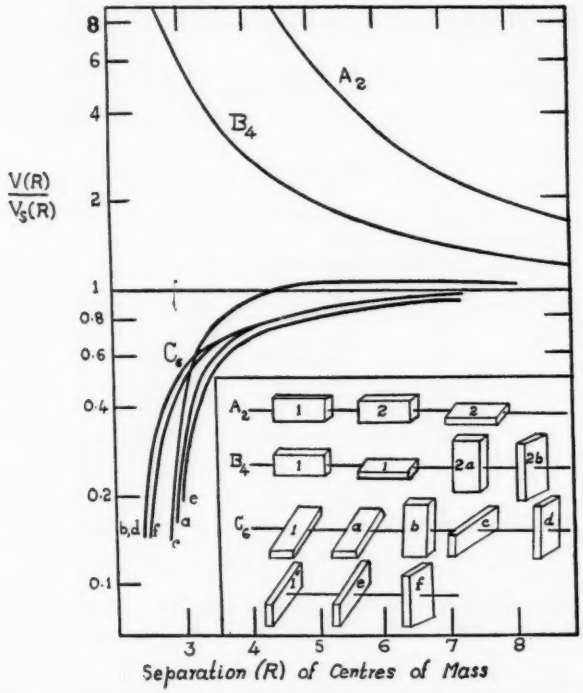

FIG. 5. Interaction energy of simulated lath-shaped particles (Ellipsoids with A : B : C = 100 : 10 : 1) relative to the interaction energy of spheres of the same volume at the same separation of centres of mass.

The two orientations represented in Curve A are derived by taking the particle (1) with each of the two marked (2). The four represented by Curve B are derived by taking each particle (1) with each of the two particles (2). While these are nearly the same as a function of R, they split into two curves as a function of δ (Fig. 6). The six orientations in the set C are derived by combining particle 1 with particles *a*, *b*, *c* and *d* and particle 1′ with particles *e* and *f* respectively.

In Fig. 6 the interaction energy of the selected shape of lath-like particles, compared with the interaction of spheres of the same volume is plotted for the same distance of closest approach of the particle surfaces. It is seen that

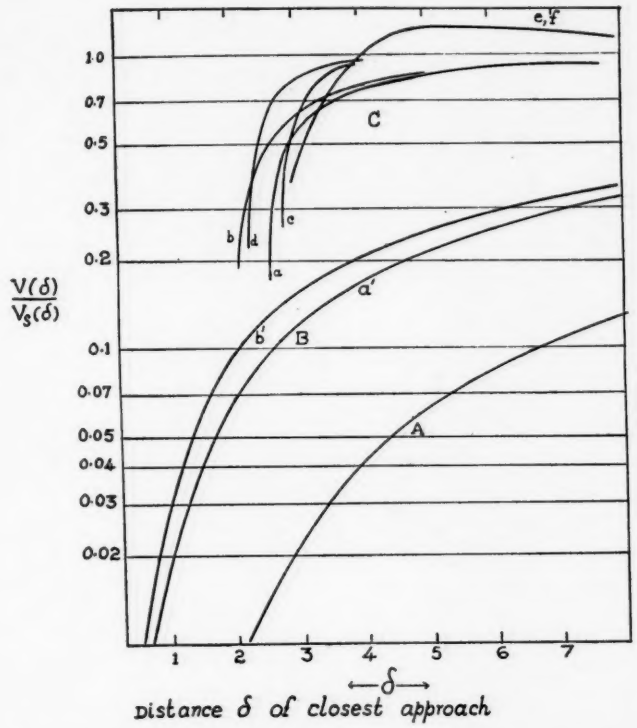

FIG. 6. Interaction energy of simulated lath-shaped particles ($a:b:c:100:10:1$) relative to the interaction energy of spheres of the same volume at the same distance of closest approach of surfaces.

for *any* orientation, the ratio decreases rapidly as the distance diminishes. Figs. 7 and 8, plotted in the same way for the rod- and disc-shaped particles, show that this is not true for all orientations, but it is uniformly true of the particular orientations which are most likely to occur, since they have the largest interaction energy at each separation of the centres of mass of the particles.

This fact explains what has been heretofore a considerable obstacle to understanding the apparent stability, that is to say, the ready mechanical

redispersibility of many sols. As the sol becomes more concentrated by settling the particles assume orientations of greatest interaction energy just through the operation of the Boltzmann factor. When the mean separation is small

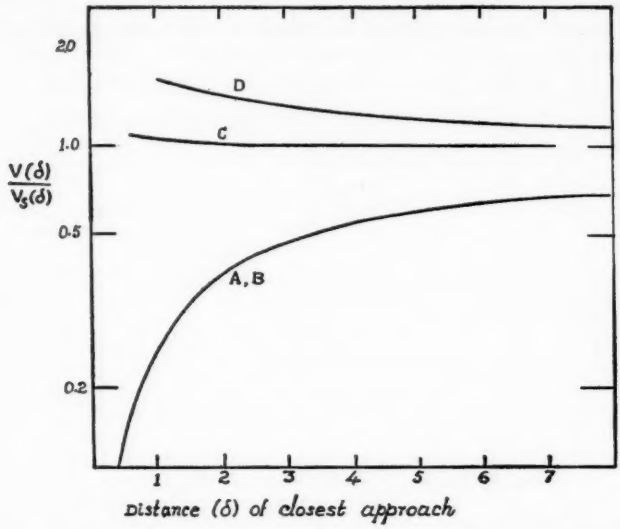

FIG. 7. Interaction energy of oblate spheroids with $a/b = 10$, relative to the interaction energy of spheres of the same volume at the same distance of closest approach of surfaces with the simulated disc-shaped particles in various orientations (see Fig. 4). δ is in arbitrary units in terms of which the product of the semi-axes of each ellipsoid is kept fixed at 0·01.

enough for the interaction to become appreciably greater than kT, or than the kinetic energy corresponding to the settling velocity, they do not settle further and hence never reach mean separations for which a huge interaction energy would be expected.

The point can be illustrated by a numerical example. In the absence of special conditions such as adsorbable long chain or polymeric stabilizing agents the solvent layer around a colloidal particle would not be more than 10 Å thick (as an order of magnitude). Even if $\wedge$ is only about 10^{-14} (a factor of 10 smaller than is often taken, and 100 times less than found by Overbeek and Sparnaay[5] for glass plates in vacuum, the interaction energy of spherical particles of 0·16 micron diameter would be $2{\cdot}6\times10^{-12}$ ergs, more than $60kT$ at room temperature, large enough to suggest the occurrence of rapid irreversible coagulation unless either the whole concept of additivity of the van der Waal's forces is wrong or unless some source of an effective repulsive force can be found. The experiments of Overbeek and Sparnaay[5] rule out

the first alternative, and several cases are now on record, even in the aqueous systems recently treated by LaMer and Smellie[4] where the second alternative seems to be ruled out also. However, rod-like particles of the anisometry used in calculating the curves of Figs. 2, 3 and 7 ($a/b = 10$) having the same volume would have an interaction energy in the most probable orientation (end-on) of only $7{\cdot}5 \times 10^{-14}$ ergs at the same separation, and hence should

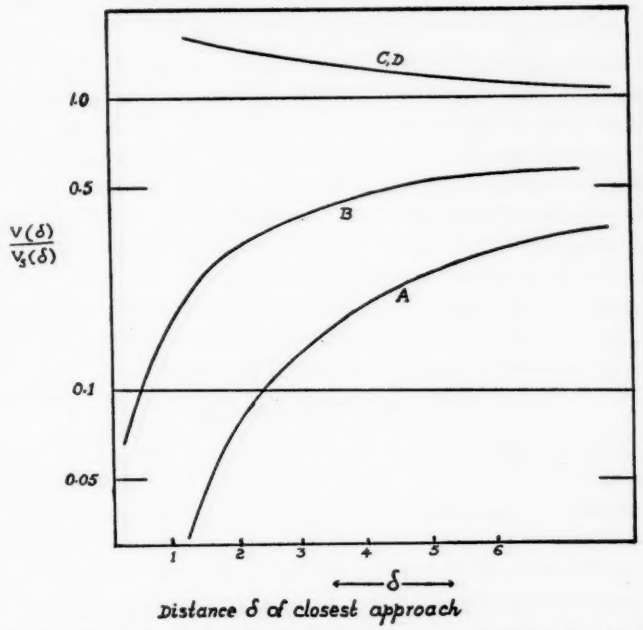

FIG. 8. Interaction energy of prolate spheroids with $a/b = 10$, relative to the interaction energy of spheres of the same volume at the same distance of closest approach of surfaces with the simulated rods in various orientations (see Fig. 2 insert).

be readily redispersible if "protected" by a 10 Å solvent layer even in the absence of steric, electrical or other unknown but much sought after mechanisms of repulsion.

It might be supposed that this interpretation is valid only for suspensions of anisometric particles. However when two isometric particles cohere, the resulting aggregate is of necessity anisometric, and hence will tend to orient itself "end-on" to a third particle with increasing extent of flocculation tending to increase the anisometry so that so long as desorption does not occur, the sol will show only mechanically reversible flocculation rather than

irreversible coagulation. The commonly observed preferential formation of chain-like aggregates of spherical particles may also be explained on this basis.

4. SUMMARY

A procedure has been developed for calculating the integrated London van der Waal's interaction energy between ellipsoidal particles in arbitrary relative orientation. Through suitable selection of axial ratios the results can be applied to real systems containing needle-shaped, plate-shaped or lath-shaped particles.

The results are applied to explain the formation of easily mechanically dispersible, flocculent suspensions of anisometric particles. For a given separation of centres of mass, the interaction energy is largest for end-to-end orientation of needles or laths and edge-to-edge orientation of plates. Hence the majority of the particles will have this orientation when their Brownian motion brings into close proximity to each other. For the limiting distances of closest approach of surfaces, of the order of one or two layers of solvent molecules, the interaction energy in this most probable orientation is insufficient to produce irreversible coagulation, even though for much less probable orientations with the longest dimensions mutually parallel the interaction energy becomes enormous at such separations.

5. ACKNOWLEDGEMENT

The author wishes to express her indebtedness to Mr. D. L. Bhattacharya and Miss D. V. Rathnamma for the results cited on electron microscopy in lithium stearate sols, and to Mr. H. N. Ramaswamy for assistance with the arithmetic calculations. Particular thanks are due to Prof. P. L. Bhatnagar of the Department of Mathematics, Indian Institute of Science, for suggesting this approach and for much help and encouragement throughout.

6. REFERENCES

1. Dube, G. P. and Das Gupta .. *Indian J. Phys.*, 1939, **13**, 411.
2. Hamaker, H. C. .. *Physica*, 1937, **4**, 1058.
3. Koelmans, H. and Overbeek, J. Th. G. *Faraday Soc. Discussions*, 1954, **18**, 52.
4. LaMer, V. K. and Smellie, R. H., Jr. *J. Coll. Sci.*, 1956, **11**, 704.
5. Overbeek, J. Th. G. and Sparnaay, M. J. *Faraday Soc. Discussions*, 1954, **18**, 12.
6. Verwey, E. J. W. and Overbeek, J. Th. G. *Theory of the Stability of Lyophobic Colloids*, Elsevier Publishing Co., 1948.
7. Vold, M. J. .. *J. Colloid Sci.*, 1954, **9**, 451.
8. ——— .. *N.L.G.I. Spokesman*, 1955, **19**, 24.

MULTIPLE SCATTERING MEASUREMENTS ON HIGH ENERGY PROTONS WITH LONG CELL LENGTHS

By S. Biswas, N. Durga Prasad and (Mrs.) S. Mitra*

(Tata Institute of Fundamental Research, Bombay)

Received May 13, 1957

(Communicated by Prof. B. Peters, F.A.SC.)

Abstract

Scattering measurements on individual tracks and relative scattering measurements on pairs of tracks have been made in two stacks exposed to 6·2 and 5·7 BeV protons respectively from the Berkeley Bevatron. Spurious scattering was determined in these two stacks for cell lengths ranging from 1 mm. to 8 mm. In one stack the magnitude of spurious scattering was very low while in the other it was fairly high. Our results indicate that:

(*a*) Spurious scattering varies with cell length t, as t^x, where x is about 0·8 for $t = 1$ mm. to 3 mm. and about 0·5 for $t = 3$ mm. to 8 mm.

(*b*) The spurious scattering is lowest near the glass surface of the emulsion and increases towards the air surface.

(*c*) The small-scale dislocations which give rise to spurious scattering extend in the plane of the emulsion at least over distances of 200 μ, but vary rapidly in size and direction with depth. Therefore, reliable relative scattering measurements require that the separation between the tracks in the depth of emulsion should be as small as possible ($\leqslant 50\,\mu$) whereas the separation in the plane of the emulsion may be as large as 200 μ.

The scattering constant for cell lengths of 1 mm. to 8 mm. has been determined. Our values are about 10% higher than the theoretical values, on the assumption that the proton energy in the Bevatron was known accurately at the time the plates were exposed.

I. Introduction

In an earlier investigation by Biswas, Peters and Rama (1955), hereinafter referred to as I, it was shown that the measurements of multiple scattering on tracks of high energy particles in nuclear emulsions are strongly influenced by the existence of small-scale dislocations which give rise to "Spurious Scattering". These results were confirmed in subsequent investigations by Fay (1955), Lohrmann and Teucher (1956), Brisbout *et al.* (1956), Apostalakis

* Now in Calcutta.

et al. (1956) and Lord *et al.* (1956). The main conclusions of all these investigations may be summarised as follows:—

1. Spurious scattering is present in all emulsions. Unlike noise, it may fluctuate widely for tracks of different particles in the same emulsion and for tracks made by the same particle in different emulsions. Therefore it is not possible to eliminate spurious scattering for *individual* tracks from a knowledge of the mean value of spurious scattering.

2. The mean value of spurious scattering differs from stack to stack. The largest and smallest mean values observed so far differ by a factor slightly smaller than two.

3. Spurious scattering varies with cell length, t, as t^x, where x is about 1·4 for " steep " tracks for t upto 1 mm. For " flat " tracks upto $t = 2$ mm., x lies between 1·0 and 0·7.

Since for flat tracks the spurious scattering increases less rapidly with cell length than true multiple scattering (which varies as $t^{3/2}$), it is possible to measure the energy of fast particles by scattering measurements using a cell size so large that spurious scattering becomes small compared to true scattering. With a cell size of 2 mm., useful scattering measurements can be made on protons of energy upto 4 BeV in a stack in which the mean value of spurious scattering is low [*e.g.*, P-stack of present work and π-stack of Brisbout *et al.* (1956)]. In a stack in which the mean value of spurious scattering is very large the upper limit of energy would be about 2 BeV for the same cell size, [*e.g.*, our N and B-stacks, I-stack of Brisbout *et al.* (1956) and the stack of Lohrmann and Teucher (1956)]. It is clear that higher energy regions become accessible to measurements by employing longer cell lengths. So far, most of the investigations have been confined to cell lengths of 2 mm. or less. There is some indication from the results of Fay (1955) and Biswas, Peters and Rama (unpublished) that spurious scattering varies less rapidly with cell size as the cell size is increased beyond 2 mm. The present investigation was undertaken to study the behaviour of spurious scattering for long cell lengths, 1 mm. to 8 mm. in order to extend the energy regions for which useful scattering measurements can be made.

It has been shown previously, in paper I, that the measurements of relative scattering (*i.e.*, the deviation of one track with respect to another track) of a closely spaced pair of tracks formed by particles of nearly equal energy yield the true energy and are free from spurious scattering effects. This method has been used extensively to determine the energy of particles where such closely spaced pairs of tracks were available. The method is applicable,

for instance, to products arising in the fragmentation of heavy primary particles of the cosmic radiation. However, the permissible separation between tracks to be used for relative scattering measurements was not known In this paper we have studied the effect of spurious scattering on relative scattering measurements. For this purpose we have investigated how the relative scattering varies with the separation of tracks both in the plane and in the depth of the emulsion.

Except for the measurement of Brisbout *et al.* who used a cell length of 2 mm., all available experimental determinations of the scattering constant refer to cell lengths of less than 1 mm. In the present work we have determined the scattering constant for longer cell lengths, 1 mm. to 8 mm.

For these investigations we have used stripped emulsion stacks exposed to 6·2 BeV and 5·7 BeV protons of the Berkeley Bevatron, the highest monoenergetic beams available at present.

II. Scattering Measurements on Tracks of 6·2 BeV Protons

2·1. *Experimental procedure.*—The emulsions used in this investigation were the two end plates of a stack of stripped emulsions, each 20 cm.× 30 cm.×600 μ, which was exposed by the Paris group [Crussard *et al.* (1956)] to the direct proton beam of energy 6·2 BeV in the Bevatron of the University of California at Berkeley. The dense core of the beam traversed the top edge of the stack, parallel to the 20 cm. side of the emulsions. The details of the exposure are given in the cited reference.

Scattering measurements were made on groups of tracks in five different regions, denoted by A, B, C, D and E. These were at different distances from the core of the beam as given below:—

Region	Distance from the core of the beam	Number of tracks measured
	cm.	
A	1·5	18
B	2·5	30
C	2·0	20
D	2·0	24
E	0	61

In regions A, B, C and D, 92 tracks were measured of total length 276 cm. (The mean length per plate was 3 cm.) In region E, in the dense core, a total track length of 72 cm. was measured. The first cell length of all tracks was at a distance of about 1 cm. from the edge of the emulsion where the beam entered the stack.

In each region, all the parallel tracks of the beam were first " mapped " by noting the X, Y and Z co-ordinates of each track at intervals of 5 mm. along the x-direction. The scattering measurements were made on each track using a basic cell length of $1000\,\mu$ and continued upto the point when the track left the emulsion or interacted. In a few cases, the track length had to be limited to 4·5 cm., the maximum length of the stage motion screw. It may be pointed that if tracks are selected on the basis that they do not deviate from their original direction by more than $50\,\mu$, some bias towards tracks which exhibit smaller scattering than the average would be introduced. The procedure adopted by us does not introduce any bias in the selection of tracks. Each track was measured twice; the repeat measurements were made at points displaced by $30\,\mu$ along the track. The reading and grain noises were eliminated as described in I.

All measurements were made with a Koristka M.S. 2 microscope. Necessary precautions were taken to keep the temperature noise to a minimum. The stage noise was measured following the procedure described in I; it was found that upto a cell length of at least 3 mm. it was negligible compared to reading and grain noise. It is reasonable to assume that the stage noise remains negligible even when 8 mm. cells are employed.

The mean reading and grain noise $\epsilon_{R,G}$ for 6·2 BeV protons was $0{\cdot}090 \pm {\cdot}001\,\mu$ and signal to noise ratio was greater than 3. The noise elimination was done in the usual way[2] for individual scattering and for relative scattering measurements. Large single scatterings were eliminated by the $4\,\overline{D}$ cut-off method[6]. For some cell lengths, scattering values were calculated also by the $4\,\overline{D}$ replacement method,† for comparison with those obtained with $4\,\overline{D}$ cut-off method. The standard deviations have been calculated assuming $\sigma = 0{\cdot}8/\sqrt{n}$ where n is the number of independent cells.

In each region of the plate the distortion of the emulsion was investigated by calculating third differences on a sample of tracks. The third difference values showed the absence of any measurable distortion for the emulsions used.

† In this procedure each signal exceeding four times $\overline{D}$, the mean of the second difference is replaced by $4\,\overline{D}$.

2.2. *Relative scattering measurements on* 6·2 *BeV protons.*—We determined the dependence of relative scattering measurements on the separation between tracks in the plane (δy) and in the depth (δz) of the emulsion (the depth refers to that in the original unprocessed emulsion). Relative scattering measurements, as functions of separation of tracks forming a pair, were carried out on pairs of tracks of the group of 30 tracks in region B. With a cell length of 1000 μ relative scattering measurements were made on independent pairs of tracks:

(i) with δz separation kept between 0 and 50 μ, and with δy separations of 0-50, 50–100, 100–150 and 150–200 μ.

(ii) with δy separation kept between 0 and 50 μ, and δz separation of 0–50, 50–100, 100–150, 150–200 and 200–300 μ.

The values are shown in Table I and are plotted in Figs. 1 (*a*) and 1 (*b*). The results show that:

(i) the relative scattering is constant for separations of tracks upto 200 μ in the plane of the emulsion (when δz is constant, 0–50 μ);

(ii) relative scattering increases rapidly as the separation between the tracks in the depth of the emulsion increases from 0–200 μ; it approaches the value of observed scattering for single tracks.

TABLE I

Variation of relative scattering with different separations between tracks in the plane, δy *and in depth* δz *of emulsion*

δz (μ) \ δy (μ)	0–50 (μ)	50–100 (μ)	100–150 (μ)	150–200 (μ)
0–50	·250±·012	·263±·020	·252±·035	·245±·033
50–100	·278±·015			
100–150	·293±·014			
150–200	·320±·020			
200–300	·322±·024			
Scattering on individual tracks	·335±·009			

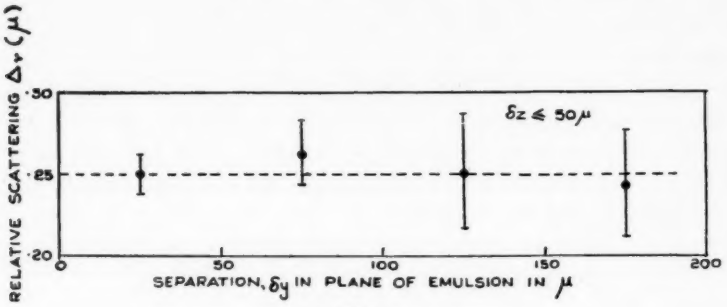

FIG. 1 (a)

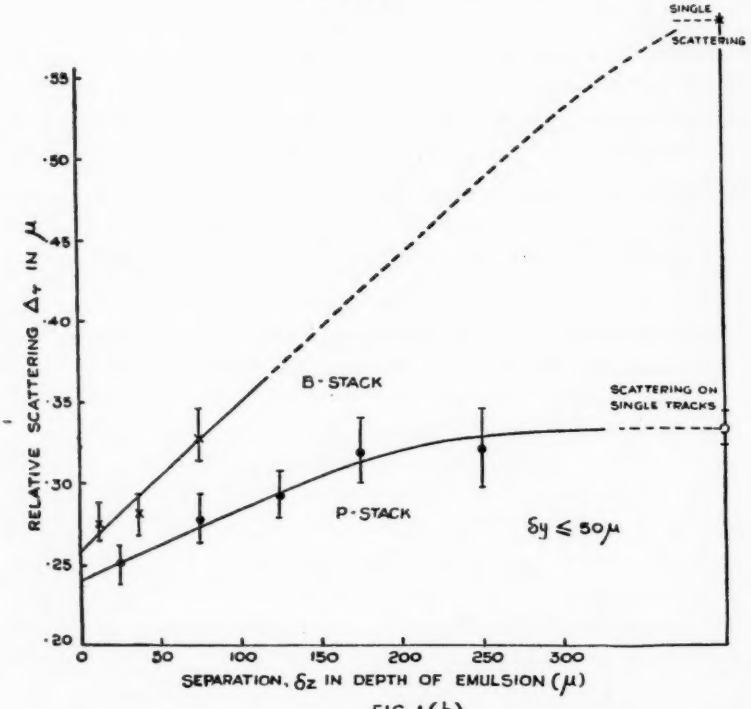

FIG. 1 (b)

FIG. 1 (*a*). Variation of relative scattering Δ_r (μ) with different separations between tracks in the plane of emulsion, δy, when separation in depth δz is between 0 and 50 μ.

FIG. 1 (*b*). Variation of relative scattering Δ_r (μ) with different separations between tracks in depth of emulsion, δz, when separation in the plane of emulsion is between 0 to 50 μ.

It was shown in paper I, that for a pair of tracks with separation less than 40 μ, the small-scale dislocations which give rise to spurious scattering are strongly correlated so that relative scattering measurements are free from spurious scattering. The present results show that strong correlations exist at least upto 200 μ separation in the plane of the emulsion, indicating that the small-scale dislocation vectors preserve magnitude and direction over distances of at least 200 μ in the plane of the emulsion. On the other hand correlations become progressively weaker for increasing separations in the depth of the emulsion. This signifies that the vector of small-scale dislocations varies rapidly from layer to layer. For $\delta z \geqslant 200\,\mu$ there is no correlation between small-scale displacement vectors.

Therefore for reliable relative scattering measurements, pairs of tracks must be selected with a δz separation as small as practicable whilst the δy separation may be as large as 200 μ. In this work we have used pairs of tracks with δy upto 200 μ and δz from 0–50 μ. The relative scattering value Δ_r' obtained with a δz separation 0–50 μ, has been extrapolated to δz equal to zero graphically [*see* Fig. 1 (*b*)]. This has the effect of reducing the measured scattering values by 4·5%. This correction factor would be larger in stacks with high spurious scattering; in B-stack which shows a very large value of spurious scattering, the correction factor would amount to ~8%.

The mean values Δ_i (obtained by multiple scattering measurements on *individual* tracks) for 92 tracks in regions A, B, C, D are shown in Table II. It also shows relative scattering values on independent pairs formed by these 92 tracks, for cell lengths ranging from 1000 μ to 8000 μ. In order to find out whether there is any difference in energy between the particles in the core and 2 cm. away from it, measurements were made using a cell length of 1000 μ on 61 tracks in the dense core (region E). There is no detectable difference in the energy of particles in the core and 2 cm. away from it; the difference, if any, is less than 2%.

2.3. *Spurious scattering in the P-stack* (6·2 *BeV protons*).—In the previous section we discussed the correlation between small-scale dislocation vectors in regions separated by distances upto a few hundred microns. In this section we discuss the dislocation vector and the spurious scattering effect which they produce. The mean value of spurious scattering Δ_{sp}, (assuming Δ_{sp} to have a gaussian distribution), can be deduced from the relation $\Delta_{sp}^2 = \Delta_{obs}^2 - \Delta_r^2$ where Δ_{obs} is the observed value of scattering on single tracks and Δ_r the mean value obtained from relative scattering measurements (extrapolated to $\delta z = 0$). Values of Δ_{sp} (for a cell length of 1000 μ) have been obtained for six different layers of the 60 μ emulsion divided in

steps of 100 μ. These values are plotted in Fig. 2; the effect is largest at the air surface and falls off towards the glass. Another stack exposed to the 5·7 BeV proton beam (to be discussed later) indicates a similar behaviour.

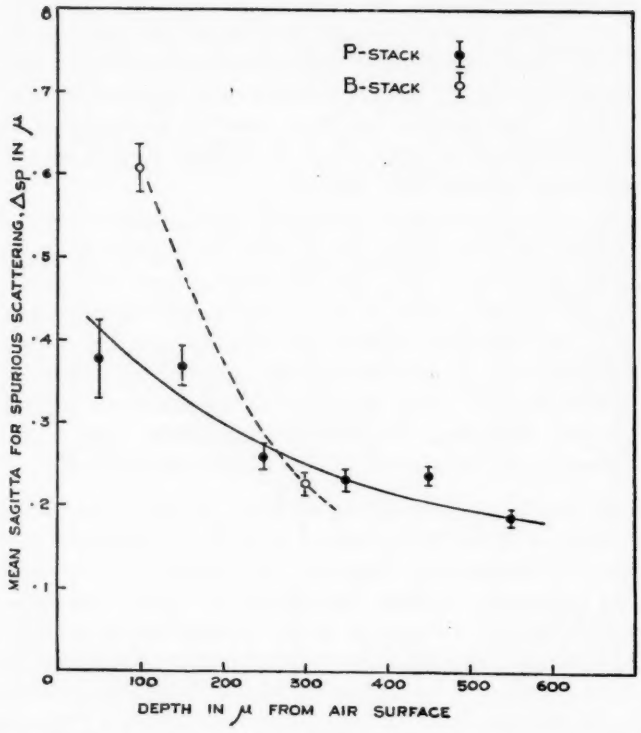

FIG. 2. Variation of the mean value of spurious scattering, $\Delta_s(\mu)$ with depth in emulsion measured from air surface.

Values of Δ_{sp} deduced for various cell lengths are shown in Table II and plotted in Fig. 3. The dependence on t can be expressed by $\Delta_{sp}=a.t^x$ where x is 0·8 for t = 1–3 mm. and $x = 0{\cdot}5$ for t = 3–8 mm. In Fig. 3, we have plotted spurious scattering values obtained by other investigators in different stacks. Spurious scattering in P-stack is low (similar to π-stack of Brisbout *et al.*). In such a stack if measurements on individual tracks are made on 4 and 8 BeV protons using cell sizes of 2 mm. and 4 mm. respectively, the energy will be under-estimated by only about 15%. In a stack which shows very high value of spurious scattering (*e.g.* N-stack and B-stack discussed later)

the corresponding proton energies would be 2 and 4 BeV for cell sizes of 2 mm. and 4 mm. respectively.

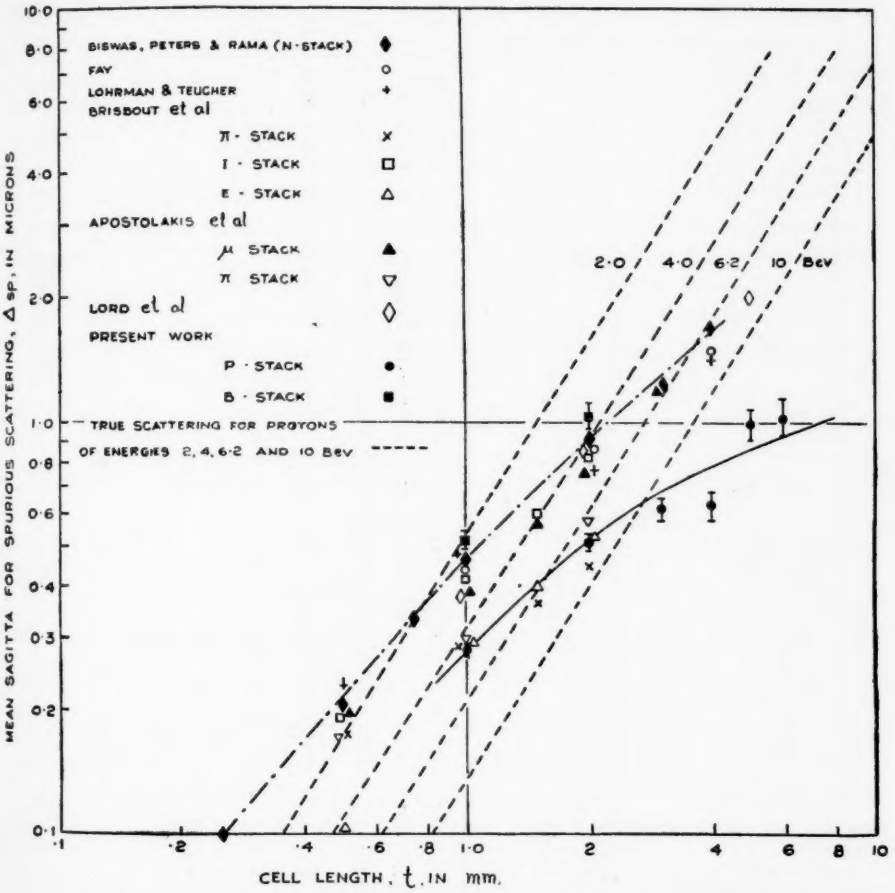
BISWAS, PETERS & RAMA (N-STACK)
FAY
LOHRMAN & TEUCHER
BRISBOUT et al
π - STACK
I - STACK
E - STACK
APOSTOLAKIS et al
μ STACK
π STACK
LORD et al
PRESENT WORK
P - STACK
B - STACK
TRUE SCATTERING FOR PROTONS OF ENERGIES 2, 4, 6·2 AND 10 BeV
2·0 / 4·0 / 6·2 / 10 / BeV
MEAN SAGITTA FOR SPURIOUS SCATTERING, Δsp, IN MICRONS
CELL LENGTH, t, IN mm.

FIG. 3. Variation of the mean value of spurious scattering Δ_{sp} (μ) with cell length in different stacks of emulsions. True coulomb scattering for protons of energies 2, 4, 6·2 and 10 BeV are shown by dotted lines. For clarity some experimental points have been slightly displaced parallel to the x-ax is.

III. MEASUREMENTS ON 5·7 BEV PROTONS (B-STACK)

Additional measurements were carried out in a stack exposed to the direct beam of 5·7 BeV protons from the Berkeley Bevatron. The stack consisted of 7 stripped emulsions, $2'' \times 4'' \times 600\,\mu$. Measurements were made

TABLE II

Multiple scattering measurements on 6·2 BeV protons (P-stack)

	Cell Length, t (μ)						
	1000	2000	3000	4000	5000	6000	8000
Individual Scattering, Δ_i (μ) ..	0·368± ·006	0·841± ·020	1·40±·04	2·05± ·08	2·92± ·12	3·84± ·19	5·80± ·37
Relative Scattering, Δ_r' (μ) ..	·251± ·007	·698± ·028	1·32±·07	2·04± ·13	2·88± ·21	3·88± ·34	5·55± ·63
Relative scattering extrapolated to zero δz separation, Δ_r (μ)	·240± ·007	·667± ·027	1·26±·07	1·95± ·13	2·75± ·20	3·70± ·32	5·30± ·60
Spurious Scattering, Δ_{sp} (μ) ..	·280± ·009	·513± ·024	0·62±·04	·63± ·05	0·99± ·08	1·03± ·11	(2·36± ·31)
Scattering Constant ($4\bar{D}$ cut-off)	30·6 ±0·9	30·1 ±1·2	30·9 ±1·7	31·0 ±2·1	31·3 ±2·3	32·2 ±2·9	(29·8 ±3·4)
($4\bar{D}$−replacement) ..	32·7 ±1·0	32·3 ±1·3	..	..	..	..	..

in three different plates and seven different regions. 124 tracks with a total track length of about 140 cm. were measured using a basic cell length of 1000 μ. The methods of individual and relative scattering measurements are as described in Section 2.1. The third difference method, used on a sample of tracks in each plate and in each region of a plate indicated absence of any measurable distortion for these emulsions. Relative scattering measurements were made for δz separations between pairs of 0–25, 25–50 and 50–100 μ as described in Section 2.2. These are shown in Fig. 1 (*b*). Values of Δ_r' obtained for $\delta z = 0$–50 μ have to be reduced by 7·5% to arrive at the extrapolated value for $\delta z = 0$. The detailed results of the scattering measurements are shown in Table III. The mean spurious scattering is much higher than that of the P-stack. The variation of the mean values of spurious scattering in different depths and with different cell lengths are plotted in Figs. 2 and 3 respectively. In this stack Δ_{sp} varied considerably from plate to plate; in one plate it was exceptionally low.

TABLE III

Multiple scattering measurements of 5·7 *BeV protons* (*B-Stack*)

	Cell length, t	
	1000 μ	2000 μ
Individual scattering Δ_i (μ)	·585 ± ·014	1·31 ± ·05
Relative scattering Δ_r' (μ)	·279 ± ·010	0·84 ± ·05
Relative scattering extrapolated to δz=0 Δ_r (μ)	·258 ± ·010	0·78 ± ·05
Spurious scattering Δ_{sp} (μ)	·525 ± ·020	1·05 ± ·07
Energy (from scattering constant of P-stack)	5·74 ± ·28	5·3 ± ·4

IV. Scattering Constant

The scattering constant, K_{CO},[6] for a 4 $\overline{D}$ cut-off has also been calculated for the various cell lengths ranging from 1 mm. to 8 mm. from the measurements on proton tracks of energy 6·2 BeV ($p\beta = 7{\cdot}02$ BeV/c.). The results are included in Table II and plotted in Fig. 4, together with the theoretical curves based on William's theory as given in the paper by Voyvodic and Pick up (1952). The latter values have been increased by 2% to include the

contribution arising from scattering by electrons. Our experimental scattering constant is about 10% higher than the theoretical values at cell lengths of 1, 2 and 3 mm. For higher cell lengths, the statistical errors are large and the values are also consistent with 10% higher scattering constant.

The higher value of scattering constant could not be attributed to higher value of scattering introduced by distortion of the emulsion, since our measurements indicated absence of any measurable distortion in our emulsions for very flat tracks used in this investigation.

The scattering constant experimentally deduced from measurements on the 6·2 BeV protons in the P-stack was used in conjunction with the relative scattering measurements on the 5·7 BeV protons in the B-stack to deduce the energy of the latter group. The value thus deduced $5{\cdot}7\pm{\cdot}3$ BeV is in good agreement with the direct measurements of the beam energy at Berkeley.

To compare our scattering constant with those of Brisbout *et al.* we have also determined the scattering constant with $4\,\overline{D}$ replacement. The values of Brisbout *et al.* (*e.g.*, $K = 27{\cdot}9\pm1{\cdot}4$ for $t = 500$–$1500\,\mu$) are in disagreement with our values ($32{\cdot}7\pm1{\cdot}0$ for $t = 1000\,\mu$).

The discrepancy of about 15% between the results of the present investigations and those of Brisbout *et al.* may be due to the effect of stage noise in the latter investigation. Brisbout *et al.* used noise elimination by the method of overlapping cells with appreciable stage noise at large cell lengths. They also measured scattering by our method of noise elimination[2] (reading and grain noise determined directly from tracks) which corresponds to a mean value of K about 10% higher than their quoted values. In our case stage noise was shown to be negligible. We determined the scattering constant by our method as well as by the method of noise elimination by overlapping cells and obtained the same values of scattering constant ($32{\cdot}7\pm1{\cdot}0$ and $32{\cdot}3\pm2{\cdot}0$) which agree within statistical error. It seems therefore that for the determination of scattering constant with long cell lengths it is necessary to use a microscope with negligible stage noise.

V. CONCLUSIONS

Our measurements on the two stacks exhibit nearly the extreme values of spurious scattering observed so far. The investigation in these stacks leads to the following conclusions on the nature of the spurious scattering:—

(*a*) It is present in all emulsions but may differ in magnitude by a factor two.

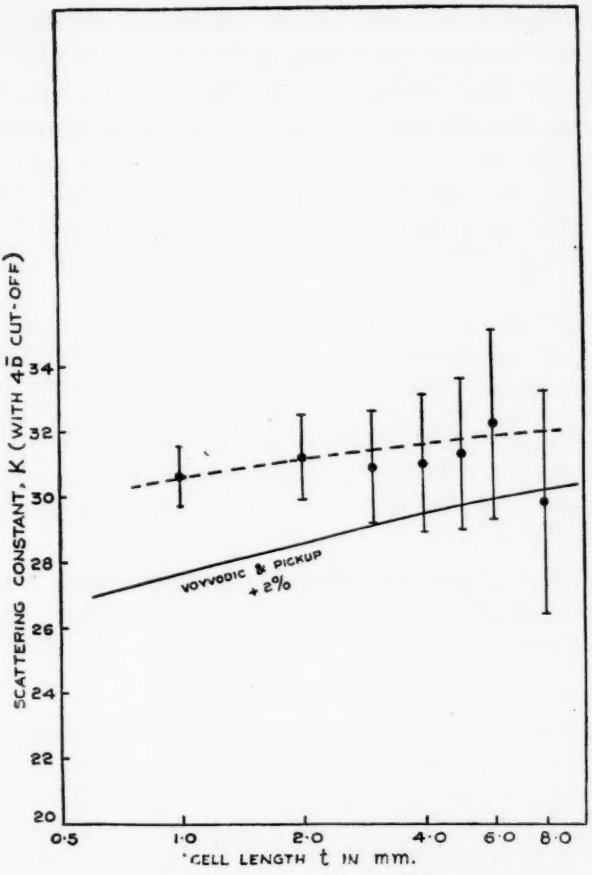

FIG. 4. Scattering constant K with 4 D cut-off as a function of cell length. The theoretical curve calculated by Voyvodic and Pickup (increased by 2% for scattering by electrons) is shown by the full line.

[*Note.*—The experimental value of K for $t = 2$ mm. is to be plotted at $30{\cdot}1 \pm 1{\cdot}2$ instead of the value shown].

(*b*) The variation of spurious scattering with cell length can be expressed as t^x where $x = 0{\cdot}8$ for $t = 1$ mm. to 3 mm. and $0{\cdot}5$ for $t = 3$ mm. to 8 mm.

(*c*) In each emulsion, which we have investigated, the magnitude of spurious scattering has its lowest value near the glass surface and increases towards the air surface.

(*d*) The small-scale dislocation vectors which give rise to spurious scattering preserve magnitude and direction over distances of at least 200 μ in the plane of the emulsion, but vary rapidly in the depth of the emulsion.

From (*d*) we find that good relative scattering measurements on pairs of tracks require that the separation in depth should be as small as practicable ($\leqslant 50\,\mu$); the separation in the plane of the emulsion can extend upto 200 μ. Relative scattering values obtained for a track separation in depth between 0–50 μ (unprocessed emulsion) have to be corrected for spurious scattering. The corrections amount to 5% and 8% for the P-stack and B-stack respectively.

From (*b*), it can be seen that with long cell lengths the contribution due to spurious scattering on measurements on individual tracks becomes small compared with true scattering. Thus in a stack with low spurious scattering (P-stack) if one uses 2 mm. and 4 mm. cell sizes it is possible to measure protons of energies upto 4 BeV and 8 BeV respectively with fair accuracy. In a stack which shows very high value of spurious scattering (*e.g.*, N-stack and B-stack) the same cell sizes can be used upto proton energies 2 BeV and 4 BeV respectively.

The scattering constant with $4\bar{D}$ cut-off, determined by us, is about 10% higher than the theoretical values given by Voyvodic and Pickup on the basis of William's theory.

ACKNOWLEDGEMENTS

We have great pleasure in expressing our thanks to Professor B. Peters for his keen interest and valuable discussions and to Dr. M. G. K. Menon for helpful suggestions during the progress of this work. We are extremely grateful to Professor L. Leprince-Ringuet of Ecole Polytechnique, Paris, for supplying us the emulsions exposed to 6·2 BeV protons, and to Professor E. J. Lofgren and Drs. G. Goldhaber and S. Goldhaber of Radiation Laboratory, Berkeley, for the emulsions exposed to 5·7 BeV protons.

REFERENCES

1. Apostolakis, A. J., Clarke, O. J. and Major, J. V. — *Nuovo Cimento*, 1957, **5**, 337.
2. Biswas, S., Peters, B. and Rama — *Proc. Ind. Acad. Sci.*, 1955, **41 A**, 154.
3. Brisbout, F. A., Dahanayake, C., Engler, A., Fowler, P. H. and Jones, P. B. — *Nuovo Cimento*, 1956, **3**, 1400.

4. Crussard, J., Fouche, V., Hennesy, J., Kayas, G., Leprince-Ringuet, L., Morellet, D. and Renard, F. *Nuovo Cimento.*, 1956, **3**, 731.

5. Fay, H. .. *Zeiss. f. Naturfor.*, 1955, **10 A**, 572.

6. Gottstein, K., Menon, M. G. K., Mulvey, J. H., O'ceallaigh, C. and Rochat, O. *Phil. Mag.*, 1951, **42**, 708.

7. Lohrmann, E. and Teucher, M. *Nuovo Cimento*, 1956, **3**, 59.

8. Lord, J. J., Chang, D. B. and Fischer, F. W. *Bull. Am. Phys., Soc.*, Series II, 1956, **1**, 250.

9. Voyvodic, L. and Pickup, E. .. *Phys. Rev.*, 1952, **85**, 91.

769–57 Printed at The Bangalore Press, Bangalore City, by C. Vasudeva Rao, Superintendent
and Published by The Indian Academy of Sciences, Bangalore.

NOTICE TO AUTHORS

Scientific papers intended for publication in the *Proceedings of the Indian Academy of Sciences* can be accepted only when they are communicated by a Fellow of the Academy whose duty shall be to satisfy himself that such communications are fit to be read at the Meeting of the Academy and published in its *Proceedings*.

Papers should not ordinarily exceed fifty pages of foolscap. MSS. should be either typewritten or written in legible hand on one side of the paper. All papers should be carefully revised by the authors and should be absolutely in final form for printing. Position for text-figures should be indicated. Each paper shall conclude with a critical summary not exceeding 350 words.

Drawings, diagrams or other illustrations should be made on larger scale (preferably) twice the size than the ones in which they are intended to appear. They should be done in Indian ink on bristol board with lettering in pencil. Scale of magnification of camera lucida tracings should be indicated by the side of drawings. In certain special cases arrangements will also be made for monochrome lithographic and other colour plates. Reduction of illustrations desired should be indicated in pencil. Appropriate legends should accompany all drawings. Names of authors are to be marked in pencil on the left-hand corner of drawing sheets. Photomicrographs should be securely mounted with colourless paste.

All tables, quotations and footnotes which will be set hereafter (beginning from Vol. I, No. 2) in types smaller than the text, should be typewritten on separate sheets and placed with the text in proper sequence. Footnotes should be numbered in Arabic numerals.

References to literature in the text should be given, whenever possible, in chronological order, only the names of authors and years of publication, in brackets, being given. They should be cited in full after the summary, the authors' names following in alphabetical order. Thus,

Name or Names of author; Name of Journal (abbreviation) with a single underline; Year of publication; Number of Volume with a double underline, and lastly page. The following would be a useful illustration:—

Bergmann and Stather . . . . . Z. Physiol. Chem., 1926, 152, 189.

Two copies of slip-proof and wherever possible, a page proof for final revision will be sent to authors. All corrections are best made on the slip-proof which should be transmitted to the Office of the Academy. All proof corrections involve heavy expenses which would be negligible if the papers are carefully revised by the authors before submission.

Fifty free reprints including plates and with cover will be supplied for each paper. Additional copies can be supplied at cost on previous intimation.

Blocks appearing in the *Proceedings* will be available for purchase by their respective authors. Orders for the same should be sent along with the corrected proofs and in any case not later than one month after the date of publication of the paper. The price charged would be 25% of the actual cost of the blocks *plus* freight and despatching charges. If the blocks are reproduced in other journals or publications, due acknowledgment should be made in them to the *Proceedings*.

The original drawings and plates of blocks appearing in the *Proceedings* will be returned to such of the authors as may require them provided the cost of despatching such originals is borne by them.

CONTENTS

PAGE

The Use of Anomalous Scattering for the Determination of Crystal Structures—$KMnO_4$ . . S. Ramaseshan, K. Venkatesan and N. V. Mani 95

Studies on the Nature of the Racemic Modifications of Optically Active Compounds in the Solid State. Part XIII. Camphor-β-sulphonyl *o*-, *m*- and *p*-nitro phenylamides (*d*- and *dl*-), camphor-β-sulphonyl *o*-, *m*- and *p*-phenylene diamines (*d*- and *dl*-) and *o*-, *m*- and *p*-phenylene-*bis*-camphor-β-sulphonylamides (*d*- and *dl*-) . . . . . Bawa Kartar Singh and Shiva Mohan Verma 112

Influence of Chemisorbed Carbon Monoxide on Subsequent Physical Adsorption of Nitrogen . . . . . V. Srinivasan 120

The Crystal Structure of Ammonium Perchlorate—NH_4ClO_4 . . . . . K. Venkatesan 134

The Crystal Structure of Potassium Perchlorate—$KClO_4$ . . . N. V. Mani 143

The Van Der Waal's Interaction of Anisometric Colloidal Particles . . . . . Marjorie J. Vold . . 152

Multiple Scattering Measurements on High Energy Protons with long Cell Lengths . . S. Biswas, N. Durga Prasad and (Mrs.) S. Mitra . . 167